Tissue-resident CD8 + T cells drive compartmentalized and chronic autoimmune damage against CNS neurons

David Frieser, Aurora Pignata, Leila Khajavi, Danielle Shlesinger, Carmen Gonzalez-Fierro, Xuan-Hung Nguyen, Alexander Yermanos, Doron Merkler, Romana Höftberger, Virginie Desestret, et al.

Title: Tissue-resident CD8$^+$ T cells drive compartmentalized and chronic autoimmune damage against CNS neurons

Authors: David Frieser[1], Aurora Pignata[1], Leila Khajavi[1], Danielle Shlesinger[2], Carmen Gonzalez-Fierro[1], Xuan-Hung Nguyen[1], Alexander Yermanos[2,3,4], Doron Merkler[4,5], Romana Höftberger[6], Virginie Desestret[7], Katharina M. Mair[8], Jan Bauer[8], Frederick Masson[1,*,†] and Roland S. Liblau[1,9, *,†]

Affiliations:

[1] Toulouse Institute for infectious and inflammatory diseases (Infinity), University of Toulouse, CNRS, INSERM, UPS; 31024 Toulouse, France

[2] Institute of Microbiology, ETH Zurich; 8093 Zurich, Switzerland

[3] Department of Biosystems Science and Engineering, ETH Zurich; 4058 Basel, Switzerland.

[4] Department of Pathology and Immunology, University of Geneva; 1211 Geneva, Switzerland

[5] Division of Clinical Pathology, Geneva University Hospital; Geneva, Switzerland

[6] Division of Neuropathology and Neurochemistry, Department of Neurology, Medical University of Vienna; Vienna, Austria

[7] National Reference Center for Paraneoplastic Neurological Syndromes, MeLiS - UCBL-CNRS, INSERM, Hôpital Neurologique, Hospices Civils de Lyon; 69500 Lyon, France

[8] Center for Brain Research, Medical University of Vienna; 1090 Vienna, Austria

[9] Department of Immunology, Toulouse University Hospital; 31300 Toulouse, France

[*] Contributed equally to this study

[†] Corresponding authors: frederick.masson@inserm.fr or roland.liblau@inserm.fr

One Sentence Summary: In mouse models of CNS autoimmunity, sustained tissue damage depends on autoreactive $CD8^+$ T cells that adopt a tissue-resident phenotype.

Abstract

The mechanisms underlying the chronicity of autoimmune diseases of the central nervous system (CNS) are largely unknown. In particular, it is unclear whether tissue-resident memory T cells (T_{RM}) contribute to lesion pathogenesis during chronic CNS autoimmunity. Herein, we observed that a high frequency of brain-infiltrating $CD8^+$ T cells exhibit a T_{RM}-like phenotype in human autoimmune encephalitis. Using mouse models of neuronal autoimmunity and a combination of T single-cell transcriptomics, high-dimensional flow cytometry and histopathology, we found that pathogenic $CD8^+$ T cells behind the blood-brain barrier adopt a characteristic T_{RM} differentiation program, and we revealed their phenotypic and functional heterogeneity. In the diseased CNS, autoreactive tissue-resident $CD8^+$ T cells sustained focal neuroinflammation and progressive loss of neurons, independently of recirculating $CD8^+$ T cells. Consistently, a large fraction of autoreactive tissue-resident $CD8^+$ T cells exhibited proliferative potential as well as pro-inflammatory and cytotoxic properties. Persistence of tissue-resident $CD8^+$ T cells in the CNS and their functional output, but not their initial differentiation, was crucially dependent on $CD4^+$ T cells. Collectively, our results point to tissue-resident $CD8^+$ T cells as essential drivers of chronic CNS autoimmunity and suggest that therapies targeting this compartmentalized autoreactive T cell subset might be effective for treating CNS autoimmune diseases.

Introduction

Chronic autoimmune diseases of the central nervous system (CNS) can target different CNS-resident cell types, including oligodendrocytes as suspected in multiple sclerosis (MS) (*1, 2*), astrocytes as identified in neuromyelitis optica spectrum disorder (*3*), or neurons in conditions such as autoimmune encephalitis, narcolepsy or autoimmune paraneoplastic syndromes (*4, 5*). An autoimmune process also appears at play in prevalent neurodegenerative disorders such as Parkinson's disease (*6*). In most CNS autoimmune diseases, the precise immune mechanisms propagating tissue damage and the resulting clinical progression remain elusive. Chronic progressive or waxing and waning inflammation is, nevertheless, a pathological hallmark of many CNS autoimmune conditions.

There is evidence that antigenic persistence is a key parameter for chronic inflammation and complete destruction of the cellular targets often results in subsiding of local inflammation (*5, 7, 8*). However, this denouement may take months or years, or cannot even be reached when the cells targeted by the autoimmune process regenerate. Continuous or repeated waves of incoming lymphocytes may contribute to the chronicity of the CNS autoimmune process. Indeed, therapies inhibiting immune cell transmigration into the CNS have reached the clinic, most notably in MS. However, therapeutic approaches targeting immune cell diapedesis have failed in progressive MS, suggesting an uncoupling of the chronic destructive autoimmune process from systemic immune responses (*9*). Indeed, in chronic inflammatory CNS diseases, a compartmentalized immune response develops, encompassing CNS-resident T cells, B cells, and myeloid cells, that is associated with progressive tissue damage (*10, 11 , 12*). Therefore, better understanding the cellular actors and mechanisms underlying the CNS-restricted immune response would be essential for the development of tailored therapeutic approaches, in particular in chronic disease stages.

Tissue-resident memory T cells (T_{RM}) have been initially described in the context of infectious diseases, as a population of long-lived memory T cells remaining in barrier tissues following the resolution of the initial infection (*13, 14*). Upon entry within the tissues, T_{RM} undergo a transcriptional program of differentiation facilitating long-term tissue residency. This program is controlled by the transcription factors Hobit and Blimp1, which inhibit expression of proteins, including Klf2, S1PR1, CCR7 and CD62L, involved in T cell tissue egress and/or homing and retention in lymphoid organs (*15*). Conversely, T_{RM} are characterized by surface markers, such as CD69, CD103, CXCR3, CXCR6, CD49a, facilitating their retention within non-lymphoid tissues. Upon tissue reinfection, T_{RM} proliferate and exhibit cytotoxic and inflammatory properties culminating in a tissue-specific anti-infectious response infection (*13, 14*).

The presence of T_{RM} has now been documented in tissues other than barrier tissues, such as the CNS (*16, 17*), and in conditions as diverse as cancer, graft-versus-host disease, allergy, and autoimmunity (*13, 18-21*). In chronic inflammatory/autoimmune diseases, such as asthma, psoriasis, vitiligo, inflammatory bowel disease, and type 1 diabetes T_{RM} have been identified in the affected tissue in animal models and/or human conditions (*19, 21, 22*). In MS, $CD8^+$ T cells expressing CD69 and CD103 represent a sizeable proportion of CNS-infiltrating T cells (*10, 23*). Recent data even suggest that T_{RM} can partake in the pathologic intrathecal immune reaction early in the disease process (*24*). Determining the role of T_{RM} in promoting chronic autoimmune CNS tissue damage is, therefore, an important challenge given their long-lasting inflammatory potential.

We identified a large fraction of $CD8^+$ T cells expressing CD103 in human brain samples from patients suffering from autoimmune diseases targeting neurons. To get further insights on the role and heterogeneity of tissue-resident $CD8^+$ T cells, and their functional interactions with other immune cell subsets in the context of autoimmune CNS tissue damage, we devised

mouse models of neuron-targeting chronic autoimmunity and made use of single-cell transcriptomics, histology, and high-dimensional flow cytometric analyses. Our data strongly suggest that tissue-resident $CD8^+$ T cells play a central role in the progressive autoimmune-mediated damage of CNS neurons.

Results

$CD8^+$ T_{RM}-like cells are detected within lesions of patients with neuron-targeting autoimmune encephalitis

To assess whether T cells expressing prototypic markers of T_{RM} cells could be detected in CNS autoimmune diseases, we performed multiplexed immunofluorescence analysis for CD3, CD8, and CD103 in lesions from ten patients with well-defined encephalomyelitis. We selected samples from four distinct conditions associated with autoantibodies directed against intracellular neuronal self-antigens (**Table S1**). In these conditions, $CD8^+$ T cells are likely responsible for neuronal damage, which can be widespread or very selective (*8, 25*). All samples were characterized by prominent T cell infiltrations within the brain parenchyma (and one dorsal root ganglion) as compared to control samples, although the T cell density varied depending on the region and the patient (**Fig. 1A-C**). On average, 60% of T cells were $CD8^+$ T cells and, among them, 50% expressed CD103 (**Fig. 1C**). CD103-expressing $CD8^+$ T cells were dispersed in the brain parenchyma and, at places, formed aggregates (**Fig. 1A-B**). Some $CD103^+$ T cells were found in close proximity to neurons (**Fig. 1D**). The high proportion of CNS-infiltrating T_{RM}-like $CD8^+$ T cells identified in human samples, prompted us to interrogate their pathogenic relevance using mouse models targeting a discrete population of CNS neurons.

Temporal association between tissue-resident CD8$^+$ T cell differentiation and progressive neuron loss in experimental CNS autoimmunity

We previously generated the Orex-HA mouse model in which orexin-producing neurons residing in the hypothalamus selectively express a model self-antigen, namely hemagglutinin (HA) from the H1N1 *influenza* virus (*26*). Upon adoptive transfer of activated (CD45.1$^+$) HA-specific CD8$^+$ T cells (**Fig. 2A**), we analyzed by flow cytometry these cells from the dissected hypothalami of Orex-HA or littermate control mice over time. The number of HA-specific CD8$^+$ T cells within the hypothalamus peaked at day 4 post-transfer, contracted at day 8, but remained relatively stable from day 15 onward (**Fig. 2B**). We next asked whether this T-cell persistence within the hypothalamus was associated with a progressive loss of orexinergic neurons and localized inflammation. To this end, orexinergic neuron counts within the hypothalamus of Orex-HA mice were assessed over time by immunohistochemistry. Orexin$^+$ neurons were progressively lost following adoptive transfer, reaching about a 70% reduction by day 30 (**Fig. 2C**). This loss was associated with an increased MHC class-II expression on microglial cells (**Fig. 2D-E**) in the dissected hypothalami.

These data indicate that an inflammatory process persisted long after the initial seeding of the antigen-specific CD8$^+$ T cells within the hypothalamus and was associated with the progressive loss of orexinergic neurons. This could be the result of the continuous recruitment of transferred antigen-specific CD8$^+$ T cells from the circulation to the hypothalamus and/or their stable residence within the CNS microenvironment, a hallmark of T_{RM}. To decipher whether HA-specific CD8$^+$ T cells could differentiate into tissue-resident CD8$^+$ T cells during CNS autoimmunity, we phenotypically characterized these cells before and after transfer into Orex-HA mice. Prior to their transfer, activated HA-specific CD8$^+$ T cells did not express CD103 (**Fig. S1A**). The hypothalamic HA-specific CD8$^+$ T cells started to co-express the canonical T_{RM} markers CD103 and CD69 by day 8 post-transfer and the proportion of T_{RM}-

like cells progressively increased, from 15.3% at day 8 to 78.5% at day 30 (**Fig. 2F-G**). The absolute number of T_{RM}-like cells in the hypothalamus remained stable from day 8 to day 30 (**Fig. 2H)**. Local antigen stimulation appeared to be necessary to mobilize HA-specific tissue-resident $CD8^+$ T cells into the hypothalamus as none was detected in the spleen of Orex-HA mice (**Fig. 2F-G**). Moreover, significantly fewer ($p<0.001$) tissue-resident $CD8^+$ T cells were found in the cerebellum, a brain region devoid of HA-expressing Orexin-neurons, and few, if any, were detected in the hypothalamus of wild-type recipient mice (**Fig. 2H, S1B**). We confirmed the parenchymal location of the hypothalamic tissue-resident $CD8^+$ T cells by injecting mice intravenously with a fluorescently labeled anti-CD8 antibody that stained endovascular $CD8^+$ T cells before collecting the brain (**Fig. 2I-J**). Immunohistochemistry confirmed the presence of $CD103^+$ $CD8^+$ T cells in the hypothalamus of Orex-HA mice and revealed instances of close apposition between T_{RM}-like cells and orexinergic neurons (**Fig. 2K)**.

Collectively, the data revealed local differentiation of antigen-specific $CD8^+$ T cells expressing T_{RM} markers during experimental CNS autoimmunity. These T cells were stably present within the hypothalamus and their presence correlated with progressive loss of neurons and sustained CNS inflammation.

Transcriptional signature of the autoreactive brain tissue-resident $CD8^+$ T cells

To further assess whether hypothalamic $CD8^+$ T cells were *bona fide* tissue-resident cells, and to investigate their role in the pathogenic mechanisms, we performed a single-cell transcriptomic analysis (scRNA-seq) of HA-specific $CD8^+$ T cells infiltrating the hypothalamus and spleen at day 30 after T-cell transfer. The hypothalamic HA-specific $CD8^+$ T cells segregated away from their splenic counterparts on the Uniform Manifold Approximation and Projection (UMAP) representation (**Fig. 3A**). Genes differentially up-

regulated in the T cells from the hypothalamus compared to the spleen were enriched in T_{RM} markers (*Itgae*, *Itga1*, *Cxcr6*, *Bhlhe40*, *Runx3*, *Junb*, *Rgs1*) and effector function associated genes (*Gzmb*, *Gzma, Ccl4, Xcl1, Ifng*) (**Fig. 3B, D**). Conversely, genes down-regulated in the hypothalamus-infiltrating $CD8^+$ T cells were involved in tissue egress (*S1pr1*, *Klf2*) and central memory T cells (*Tcf7*, *Sell*, *Ccr7*) (**Fig. 3B, D**). Gene set enrichment analysis (GSEA) further confirmed that the transcriptome of HA-specific hypothalamic $CD8^+$ T cells in comparison to their splenic counterparts is strongly enriched for a previously published brain T_{RM} gene signature (*27*) (**Fig. 3C**).

Additionally, we validated the transcriptomic data by flow cytometry. The expression of T_{RM}-associated markers CXCR6, CXCR3, and CD49A (encoded by *Itga1*) were increased in hypothalamic HA-specific $CD8^+$ T cells compared with their splenic counterparts, at day 30 post-transfer (**Fig. S2**). Conversely, Ly-6c expression associated with vascular/recirculating T cells was decreased in hypothalamus-infiltrating T cells similarly to the transcription factors T-BET and EOMES (**Fig. S2**), which interfere with T_{RM} development. Moreover, analysis of GRANZYME B (**Fig. 3E)**, IFNγ and TNF (**Fig. 3F-G**) expression confirmed the high effector potential of hypothalamic HA-specific tissue-resident $CD8^+$ T cells. As local cognate antigen expression has been shown to be an important mechanism of T_{RM} maintenance within the tissues (*28, 29*), we assessed whether HA-specific tissue-resident $CD8^+$ T cells were proliferating locally. In line with a potential reactivation of HA-specific tissue-resident $CD8^+$ T cells within the hypothalamus, on average 19.4% of these hypothalamic T cells expressed the proliferation marker KI-67 at day 30, whereas splenic HA-specific T cells were almost invariably negative, and only 3.6% of hypothalamic host $CD8^+$ T cells expressed KI-67 (**Fig. 3H**).

Taken together, these results confirmed the T_{RM} differentiation status of hypothalamus-infiltrating HA-specific $CD8^+$ T cells and demonstrated that these cells proliferated and exhibited an effector phenotype within the brain microenvironment.

Tissue-resident $CD8^+$ T cells infiltrating the hypothalamus are phenotypically and functionally heterogeneous

Next, we asked whether the tissue-resident $CD8^+$ T cells represented a homogenous population or rather encompassed different subsets exhibiting different functions. Clustering analysis of the scRNA-seq data uncovered nine different clusters in HA-specific $CD8^+$ T cells isolated from spleen and hypothalamus at day 30 post-transfer, including three clusters, namely 1, 5 and 8, specific to the hypothalamus (**Fig. 4A-B; Fig. S3A**). A GSEA analysis showed that all three hypothalamic clusters exhibited a strong enrichment in brain T_{RM} gene signature (**Fig. 4C, Fig. S3B-C**).

As chronic antigenic stimulation could trigger an exhaustion program of differentiation, we then evaluated whether the three hypothalamic clusters exhibited such signature. The GSEA revealed that clusters 5 and 8 were also enriched for an exhausted T-cell signature (**Fig. 4C, Fig. S3B**). However, cluster 5 distinctively up-regulated co-inhibitory receptors classically associated with exhausted T cells such as *Pdcd1*, *CD160*, *Lag3* (**Fig. 4D**) and *Havcr2*. By contrast, the exhaustion gene signature of cluster 8 appeared linked to the type I IFN signaling pathway (*Igs20, Ifit1, Ifit3, Ifit3b Ifitm3, Ifi203, Ifi27l2a*). Accordingly, GSEA analysis for IFN gene signature of the 3 clusters confirmed that DE genes in cluster 8 were strongly enriched in type I IFN gene signaling including *Bst2, Ly6a, Irf7*, and *Stat1* (**Fig. 4C,E**). Clusters 1 and 8 were characterized by cells with the highest expression of cytotoxic molecules (*Gzma*, *Gzmb*). By contrast cells from Cluster 5 had a lower cytotoxic potential,

but the highest cytokine and chemokines expression (*Ifng, Xcl1*, *Ccl4*) despite the expression of exhaustion markers (**Fig. 4D**).

To further validate these 3 clusters, we analyzed expression of distinctive surface markers on hypothalamic and splenic HA-specific T cells by high-dimensional flow cytometry, at day 30 post-transfer. This analysis confirmed the heterogeneity of the hypothalamic HA-specific tissue-resident $CD8^+$ T cells (**Fig. 4F**). Unsupervised clustering of HA-specific $CD8^+$ T cells from spleen and hypothalamus identified 8 clusters, of which 5 (clusters 3, 4, 6, 7 and 8) were specific to the hypothalamus (**Fig. 4G**). The analysis of the markers associated with these 5 hypothalamic clusters matched those from the scRNA-seq data. Cluster 6 expressed exhaustion markers including TOX, LAG3, PD-1 and TIM-3 and the proliferation marker KI-67. Cluster 4 was characterized by a high expression of GRANZYME B, LAG3 and PD-1 but absence of other exhaustion markers. Finally, clusters 3 and 7 appeared to be related to the IFN signature identified by scRNAseq, as shown by the high co-expression of BST2 and LY-6A (SCA-1), variable expression of GRANZYME B and low expression of TOX and PD-1 (**Fig. 4F-G, Fig. S3D**).

To understand which cluster could be the main driver of neuronal loss, we measured expression of cytokines and cytotoxic molecules by the three tissue-resident $CD8^+$ T cell clusters. This analysis revealed that the PD-1-expressing tissue-resident $CD8^+$ T cell subsets (TOX^+ and TOX^-) expressed the highest amount of IFNγ, with the $PD\text{-}1^+$ TOX^- subset showing a greater proportion of both IFNγ/TNF and PERFORIN/GRANZYME B double producers (**Fig. S3E-F**). These data suggest that the two PD-1-expressing tissue-resident $CD8^+$ T cell subsets are likely implicated in neuronal loss.

Altogether this analysis revealed that autoreactive tissue-resident $CD8^+$ T cells infiltrating the CNS are phenotypically and functionally heterogeneous.

Autoreactive brain tissue-resident CD8$^+$ T cells also develop after vaccine-induced autoimmunity

To assess whether the tissue-resident differentiation of HA-specific CD8$^+$ T cells within the brain resulted from their in vitro activation conditions, we used a different autoimmune model of neuroinflammation involving in vivo T cell priming (*30*). Here, Orex-HA mice are co-transferred with naïve HA-specific CD8$^+$ T cells and naïve HA-specific CD4$^+$ T cells and are immunized the next day with the Pandemrix influenza vaccine (**Fig. 5A)**. This vaccine was associated with narcolepsy side-effect in humans following the 2009-2010 H1N1 influenza vaccination campaign. Importantly, this vaccine contains the immunogenic K^d-restricted and I-E^d-restricted HA peptides recognized by the HA-specific CD8$^+$ and CD4$^+$ T cells, respectively. In this model, vaccination-induced activation of HA-specific T cells resulted in a robust hypothalamic T-cell infiltration **(Fig. 5B)** and progressive loss of orexinergic neurons, reaching 36% by 30 days post-vaccination **(Fig. 5C)**, associated with sustained inflammation with presence of MHC-II$^+$ activated microglia cells (**Fig. S4A-B**).

The HA-specific CD8$^+$ T cells peaked in the hypothalamus of Orex-HA mice 2 weeks after vaccination and persisted for more than 8 weeks, again suggesting a potential T_{RM}differentiation (**Fig. 5B**). The proportion of HA-specific CD8$^+$ T cells expressing CD69 and CD103 in the hypothalamus increased from 42.4% 2 weeks after vaccination to 68.8% at 8 weeks (**Fig. 5D-F**). Their splenic counterparts did not harbor this phenotype (**Fig. 5D-E**), suggesting that the CNS tissue and/or presence of the HA antigen was instrumental for T_{RM}-like differentiation. HA-specific CD8$^+$ T cells selectively exhibited the T_{RM}features whereas the endogenous CNS-infiltrating CD8$^+$ T cells mostly did not (**Fig. S4C**).

Transcriptome analysis (bulk RNA-seq) at day 14 after vaccination confirmed that HA-specific CD8$^+$ T cells infiltrating the hypothalamus adopted a T_{RM} transcriptional program. Indeed, the set of genes differentially expressed between hypothalamic compared to splenic

HA-specific $CD8^+$ T cells was highly enriched for brain T_{RM} gene expression signature (**Fig. 5G**).

Moreover, gene expression analysis suggested that in vivo priming of HA-specific $CD8^+$ T cells led to a similar functional outcome as in the adoptive transfer model. We observed an up-regulation of genes encoding T_{RM} canonical markers (*Itgae*, *CD69*, *P2xr7*, *Bhlhe40*), exhaustion markers (*Pdcd1*, *Lag3*, *Tox*), effector cytokines (*Ifng*, *Tnf*, *Ccl4*, *Xcl1*), cytotoxic molecules (*Gzmb, Gzmc*) and IFN signaling associated genes (*Ly6a, Bst2, Stat1, Irf7*) in the hypothalamus-derived cells and a reciprocal down-regulation of genes involved in T cell tissue egress (*Klf2, S1pr1*) and central memory differentiation (*Tcf7, Id3, Sell*) (**Fig. 5H**). Akin to the adoptive transfer model, hypothalamic HA-specific $CD8^+$ T cells primed by Pandemrix vaccination were more cytotoxic and proliferative as shown by the increased expression of GRANZYME B and KI-67, respectively (**Fig. S4D-E**).

These data indicate that autoreactive tissue-resident $CD8^+$ T cells with effector potential can form early on in the CNS in the setting of a vaccine-induced neuroinflammatory disease and are associated with sustained inflammation and loss of orexinergic neurons.

Recirculating HA-specific effector $CD8^+$ T cells are dispensable for orexin-neuron loss

To investigate the relative contribution of the recirculating compared to hypothalamus-resident HA-specific $CD8^+$ T cells in the loss of orexinergic neurons we depleted circulating $CD8^+$ T cells using an anti-CD8α depleting antibody starting 8 days after adoptive transfer of activated HA-specific $CD8^+$ T cells (**Fig. 6A**). This treatment resulted in a sustained and almost complete elimination of peripheral HA-specific $CD8^+$ T cells (**Fig. 6B-D; Fig. S5A**). However, the proportion and total number of HA-specific tissue-resident $CD8^+$ T cells in the hypothalamus were not reduced by the peripheral $CD8^+$ T cell depletion at day 30 (**Fig. 6E-G, Fig. S5B**) and up to day 90 (**Fig. S5C**) post-transfer, demonstrating that these tissue-resident

$CD8^+$ T cells are long-lived, stably maintained within the hypothalamus of Orex-HA mice and are not dependent on replenishment from peripheral T cells.

Neither the microglial activation (**Fig. 6H**) nor the loss of orexinergic neurons (**Fig. 6I**) were significantly affected ($p>0.05$) by the depletion of circulating $CD8^+$ T cells. Altogether, these data demonstrate that recirculating $CD8^+$ T cells are not required for the progressive loss of orexinergic neurons and the sustained focal neuroinflammation, and suggest that tissue-resident $CD8^+$ T cells are key for inflammatory tissue damage.

$CD4^+$ T cell-mediated maintenance of tissue-resident $CD8^+$ T cells is required for neuron loss and sustained local inflammation

$CD4^+$ T cell help is important for the development and/or the maintenance of T_{RM}in infection models (*31-33*). Therefore, we postulated that depletion of $CD4^+$ T cells in our mouse model would deplete tissue-resident $CD8^+$ T cells, allowing to assess their role in autoimmune disease chronicity. $CD4^+$ T cells were thus depleted starting 5 days prior to adoptive transfer of HA-specific $CD8^+$ T cells. To rule out a potential role for peripheral $CD8^+$ T cells in that setting, we also combined $CD4^+$ T cell depletion with $CD8^+$ T cell depletion (starting from day+8, after seeding of the tissue-resident $CD8^+$ T cells within the hypothalamus) (**Fig. 7A**). $CD4^+$ T cells were absent from the periphery and CNS throughout the experiment following administration of depleting anti-CD4 antibody (**Fig. 7B-C**; **Fig. S6A**). The $CD4^+$ T cell depletion did not reduce the migration of HA-specific $CD8^+$ T cells to the hypothalamus at day 8 after transfer (**Fig. 7D**) nor did it prevent their differentiation into $CD69^+$ $CD103^+$ T cells (**Fig. 7E**). At this early time-point, the magnitude of microglial cell activation in the hypothalamus was not altered by $CD4^+$ T cell depletion (**Fig S6B**). However, at day 30 the number of tissue-resident $CD8^+$ T cells was strongly reduced upon combined $CD4^+$ (from day-5) and $CD8^+$ (from day+8) T cell depletion compared to the other conditions (**Fig. 7F**),

suggesting that $CD4^+$ T cell depletion affected the persistence of tissue-resident $CD8^+$ T cells in the CNS but not their initial differentiation.

To further explore the contribution of $CD4^+$ T cell help on the phenotype and functions of tissue-resident $CD8^+$ T cells, we used high-dimensional flow cytometric analysis and determined whether the distribution of tissue-resident HA-specific $CD8^+$ T cells within the previously-identified hypothalamic clusters could be affected by the depletion of $CD4^+$ T cells alone (**Fig. 7G-H**) or combined with the depletion of $CD8^+$ T cells in the periphery (**Fig. S6C**). Cluster 5 (the more cytotoxic PD-1^{int} GRANZYME B^{high} subset) and cluster 9 (the exhausted TOX^+ PD-1^+ $TIM3^+$ KI-67^+ cells) were selectively reduced by $CD4^+$ T cell depletion combined or not with $CD8^+$ T cell depletion (**Fig. 7G-H; Fig. S6C-D**). By contrast, the proportion of cells in clusters 1 and 4, comprising poorly cytotoxic tissue-resident $CD8^+$ T cells expressing LY-6A and BST-2 (mostly PD-1^- TOX^-), was increased upon $CD4^+$ T cell depletion (**Fig. 7G, Fig. S6C-D**). These data indicate that $CD4^+$ T cell depletion impacted both the maintenance and the function of hypothalamic tissue-resident $CD8^+$ T cells.

Moreover, the combined depletion of $CD4^+$ and $CD8^+$ T cells affected local inflammation and neuronal loss. Indeed, the proportion of MHC-II^+ microglial cells strongly correlated with tissue-resident $CD8^+$ T cell numbers (**Fig. 7I**). Orexinergic neurons were partly preserved in Orex-HA mice in the $CD4^+$ and $CD8^+$ T cell double-depleted group (**Fig. 7J**). Therefore, the data suggest that the $CD4^+$ T cell-mediated control of long-term persistence and function of tissue-resident $CD8^+$ T cells within the CNS is essential to drive the chronicity of the autoimmune process.

Next, the phenotype of the host $CD4^+$ T cells from dissected hypothalamus and spleen of Orex-HA mice was investigated by high-dimensional flow cytometry, 30 days after $CD8^+$ T cell transfer. Among the 9 different $CD4^+$ T cell clusters identified, cluster 4 represented the dominant hypothalamic subset (24.9%) (**Fig. S7A**). This cluster expressed markers of both

tissue residency (CXCR6^{high} CD49A^{high}, CD69^{+}) and T follicular helper cells (T_{FH}) (CXCR5^{+}, PD-1^{+}, ICOS^{+}) (**Fig. S7B-D**), resembling the tissue-resident helper cells (T_{RH}) (*33*). To assess whether this cluster could contribute locally to the maintenance of tissue-resident CD8^{+} T cells we enumerated HA-specific tissue-resident CD8^{+} T cells in the hypothalamus of Orex-HA mice depleted of peripheral CD4^{+} T cells 5 days prior to CD8^{+} T cell transfer (early depletion) or at day 8 post-transfer (late depletion). At day 8, host CD4^{+} T cells are already detected in the hypothalamus and we reasoned that systemic injection of depleting anti-CD4 mAb should spare tissue-resident CD4^{+} T cells while eliminating peripheral/recirculating CD4^{+} T cells. Additionally, peripheral CD8^{+} T cells were depleted from day 8 onward to avoid potential contributions from peripheral CD8^{+} T cells (**Fig. S7E**). As expected, CD4^{+} T cells were absent from the spleen in both early and late CD4^{+} T cell depletion and from the hypothalamus upon early depletion (**Fig. S7F**). However, late CD4^{+} depletion spared a population of CD4^{+} T cells in the hypothalamus expressing CD69, CD49A, and CXCR6, confirming their tissue-resident phenotype (**Fig. S7G-I**). Additionally, we confirmed that a large majority (on average 81.6%) of these CD4^{+} T cells co-expressed T_{FH} markers (**Fig. S7J-K**). In contrast to early CD4-depletion, late depletion did not impair tissue-resident CD8^{+} T cell maintenance, suggesting that local help provided by the tissue-resident CD4^{+} T cells allows persistence of tissue-resident CD8^{+} T cells (**Fig. S7L**). This conclusion is supported by microscopy observations of host CD4^{+} T in close vicinity with CD103^{+} tissue-resident CD8^{+} T cells within the hypothalamus (**Fig. S7M**).

We, then, addressed whether the host CD4^{+} T cells could be activated in secondary lymphoid organs by antigen leakage resulting from the destruction of HA-expressing neurons. When transferred into Orex-HA or control mice that had received in vitro activated HA-specific CD8^{+} T cells 12 days earlier, CTV-labelled naïve HA-specific CD8^{+} and CD4^{+} T cells proliferated three days later in the cervical LNs, and to lesser extent in spleen, of Orex-HA

mice (**Fig. S8A-B)**. This antigen leakage allowed activation of naïve HA-specific T cells as indicated by higher expression of activation markers in Orex-HA compared to control mice (**Fig. S8B-C**).

Taken together our results suggest that (i) tissue-resident $CD4^+$ T cell provide local help to tissue-resident $CD8^+$ T cells, thereby allowing their long-maintenance, and (ii) that some of these $CD4^+$ T cells are primed by neuronal antigen leakage induced by the first wave of brain-infiltrating autoreactive $CD8^+$ T cells.

$CD8^+$ T cells within lesions of patients with neuron-targeting autoimmune encephalitis express markers present in mouse tissue-resident $CD8^+$ T cells.

To further link the mouse data with human pathology, we performed additional brain immuno-histological staining in patients with autoimmune diseases against intracellular neuronal self-antigens, combining the CD8 and CD103 staining, with CD69, GRANZYME B, TOX, BCL2 and PD-1 staining (**Fig. 8A-E**). CD69 and BCL2 were highly and preferentially expressed in $CD8^+$ T cells expressing CD103, further underlining their tissue-resident feature (**Fig. 8F**). Moreover, human CNS-infiltrating $CD103^+$ $CD8^+$ T cells also frequently expressed some key molecules delineating specific tissue-resident $CD8^+$ T cell subsets in our mouse study, such as GRANZYME B, TOX and PD-1 (**Fig. 8F**). It is, therefore, possible that, as in the mouse model, these tissue-residing $CD8^+$ T cells are the drivers of neuronal destruction in human pathologies.

Discussion

In this study, we analyzed brain tissue from patients with CNS neuron-targeting autoimmune diseases and identified a high proportion of $CD8^+$ T cells expressing CD103, a prototypic T_{RM} marker. We then made use of a mouse model of autoimmunity against CNS neurons to

investigate the contribution of tissue-resident $CD8^+$ T cells in the disease process. We showed that CNS-infiltrating autoreactive effector $CD8^+$ T cells rapidly acquired a tissue-resident phenotype, remained for months, independently of any supply from the periphery. These cells fueled locally the deleterious autoimmune process resulting in 'brain-autonomous' neuronal degeneration. Tissue-resident $CD8^+$ T cells critically relied on $CD4^+$ T cells for their persistence in the CNS, for their cytotoxic properties, and for the progressive autoimmune–mediated neuronal loss. These data suggest that autoreactive tissue-resident $CD8^+$ T cells have a direct deleterious effect on the self-antigen-expressing neurons and are needed for the chronicity of the disease process.

The concept of the immune privilege of the CNS has been challenged by the identification of several gateways between the peripheral immune system and the brain, despite the restrictive blood-brain barrier (*34, 35*). In addition, the CNS may enable the differentiation and the survival of tissue-resident immune cells stably lodged in situ. This would explain why human chronic inflammatory diseases of the CNS are frequent, ranging from autoimmune, to neurodegenerative or infectious. Recent data from single-cell RNA sequencing of human CSF cells from patients with MS and healthy donors indicate that local memory $CD8^+$ T cells, but also a cluster of memory $CD4^+$ T cells, express markers of tissue residence as well as cytotoxicity-related genes (*24, 36*). These $CD8^+$ T cells, the clonally expanded ones, share expression of αE integrin, CD69, CXCR6, and CCR5, suggesting possible therapeutic targeting (*24, 36*).

T_{RM} have been involved in pathogen clearance and/or in the control of pathogen reactivation in infectious diseases of the CNS (*31, 32, 37, 38*). By contrast, T_{RM} phenotype and function have been scarcely documented in the context of CNS autoimmune diseases and it is unclear whether T_{RM} are sustaining the chronicity of neuroinflammatory diseases. Indeed, although T_{RM}-like cells have been reported in the active lesions of MS patients (*10, 23*), and in

Parkinson's disease (*39*) their contribution to pathology and their antigenic specificity are still elusive. In addition, whether T_{RM} could be found in other $CD8^+$ T cell-mediated autoimmune diseases of the CNS is unknown. To tackle these issues, we analyzed the presence of T_{RM}-like cells in brain tissue of patients suffering from severe autoimmune diseases, characterized by $CD8^+$ T cell-mediated autoimmune targeting of neurons. Interestingly, a high density of T_{RM}-like cells was found in these samples, suggesting that T_{RM} differentiation is likely a hallmark of these conditions.

We showed, in an experimental model, that antigen-specific tissue-resident $CD8^+$ T cells formed rapidly after their entry in the CNS and resided in the hypothalamus for up to 3 months. Critically, the presence of tissue-resident $CD8^+$ T cells was associated with the progressive loss of orexinergic neurons over time, which correlated with microglial activation. Conversely, depletion of peripheral $CD8^+$ T cells did not prevent loss of the orexinergic neurons, indicating that, once the tissue-resident $CD8^+$ T cells are established, peripheral $CD8^+$ T cells are dispensable. Higher numbers of tissue-resident $CD8^+$ T cells were present in the hypothalamus than cerebellum, a site devoid of orexinergic neurons, indicating that antigen presentation is essential for the compartmentalized accumulation of tissue-resident $CD8^+$ T cells.

To decipher whether tissue-resident $CD8^+$ T cells were directly involved in the loss of neurons and in the long-lasting compartmentalized inflammatory process, we depleted $CD4^+$ T cells prior to the HA-specific $CD8^+$ T cell transfer. Indeed, $CD4^+$ T cells had been shown to promote T_{RM} differentiation and/or survival in infectious settings (*31-33*). Our data revealed that when $CD4^+$ T cell depletion was combined with peripheral CD8 T cell depletion, hypothalamic tissue-resident $CD8^+$ T cells numbers were drastically reduced, and reciprocally, orexin neurons were partially protected. However, $CD4^+$ T cell depletion alone did not reduce the number of tissue-resident $CD8^+$ T cells. A possible explanation is that in

the absence of help from $CD4^+$ T cells, tissue-resident $CD8^+$ T cells are unable to persist but are progressively replaced by peripheral $CD8^+$ T cells refilling the niche left free by 'unhelped' $CD8^+$ T cells. These results are congruent with experimental brain infection with Poliomavirus in which virus-specific T_{RM} were unable to persist in the combined absence of peripheral $CD8^+$ T cells and of IL-21-producing $CD4^+$ T cells expressing T_{FH} surface markers (*31, 32*). The $CD4^+$ T cell subset likely providing help to tissue-resident $CD8^+$ T cells in the brain expressed T_{FH} surface markers as well as tissue-resident phenotype, as described in the lung following influenza virus infection (*33*). The priming of $CD4^+$ T cells could be secondary to the neuronal damage caused by the first wave of autoreactive $CD8^+$ T cells, leading to neuronal antigen leakage in the cervical LNs. This suggests that chronic CNS inflammation could be fueled by a positive feedback loop in which neuronal destruction by $CD8^+$ T cells leads to de novo priming of $CD4^+$ T cells promoting, in turn, the long-term persistence and effector functions of tissue-resident $CD8^+$ T cells.

In the context of autoimmunity, a key question is how to best target the T_{RM} compartment for therapeutic purposes. Indeed, as peripheral T cells can replace T_{RM}, both peripheral and tissue-resident compartments need to be considered. A recent report has detected, among the pool of peripheral memory precursor cells, precursors of T_{RM}, which exhibit an increased ability to form de novo T_{RM} (*40*). One could speculate that both the peripheral T_{RM} precursors and the mature CNS T_{RM} should be targeted for durable elimination of pathogenic autoreactive T_{RM}. Interestingly, anti-CD20 mAbs, one of the most efficient treatment of MS, not only deplete CD20-expressing B cells but also CD20(dim)-expressing $CD8^+$ T cells in the peripheral blood (*41*). $CD20^{dim}$ T cells infiltrating MS lesions are strongly enriched in cells expressing T_{RM} markers ($CD69^+$ $CXCR6^+$) (*42*). It remains possible that the depletion of these CD20-expressing T_{RM} or their peripheral precursors might contribute to the efficacy of anti-CD20 therapy.

To further characterize the phenotype and function of hypothalamic tissue-resident $CD8^+$ T cells, we combined single-cell RNA transcriptomic analysis and high-dimensional flow cytometric analysis. These approaches uncovered the heterogeneity of the hypothalamic tissue-resident $CD8^+$ T cells, encompassing three phenotypically and functionally distinct clusters. The first cluster was characterized by high expression of the cytotoxic molecule GRANZYME B. Conversely, cells from the second cluster were poorly cytotoxic, expressed multiple exhaustion-associated molecules (TOX, PD-1, TIM-3), the proliferation marker KI-67 and the effector molecule IFNγ. Finally, we uncovered a cluster of tissue-resident $CD8^+$ T cells characterized by high expression of many type I IFN responsive genes. We observed that the proportion of both the 'GRANZYME B^+' and 'TOX^+' clusters were substantially reduced upon early $CD4^+$ T cell depletion whereas the 'IFN I signaling' cluster reciprocally increased. Although TOX expression can control T cell exhaustion during chronic LCMV infection (*43*), it is also induced after TCR activation similar to PD-1 and Tim3 and has recently been described as a determinant of the encephalitogenic potential and persistence of self-reactive $CD8^+$ T cells in experimental CNS autoimmunity (*43*).

With the recent advance in single-cell transcriptome profiling, it has becoming clearer that T_{RM} form a heterogeneous T cell pool and that the residency program does not prevent T cells from acquiring specialization programs (*44*). The mechanisms underpinning T_{RM} heterogeneity are still poorly understood although the type of antigen-presenting cells (APCs) restimulating T_{RM} within the tissue has been shown to influence their transcriptional programming. Indeed, antigen presentation by non-hematopoietic cells to T_{RM} in the lungs during an influenza virus infection was associated with repression of type I IFN inducible genes and, conversely, an increased expression of *Ifnγ*, *Xcl1* or *Ccl4* (*29*), all highly expressed by the 'TOX^+' tissue-resident $CD8^+$ T cell cluster in our model. We propose that heterogeneity observed among hypothalamic tissue-resident $CD8^+$ T cells could reflect direct

antigen presentation by neurons compared to cross-presentation by professional APCs migrating to the brain.

Our study, together with the companion article (45), demonstrates the important contribution of tissue-resident $CD8^+$ T cells to the chronicity of destructive CNS autoimmune experimental disease. Moreover, $CD8^+$ T cells harboring a T_{RM}-like phenotype and expressing key functional molecules uncovered in the mouse models were prevalent within brain tissues of patients suffering from neuron-targeting autoimmune diseases.

Limitations from our study include the fact that the autoreactive potential of the human T_{RM}-like cells was not investigated, although their high expression of GRANZYME B and PD-1 suggests recent antigenic stimulation rather than bystander activation. Moreover, we have not explored, in the mouse model, whether the priming phase of autoreactive CD8 T cells can impact their differentiation into T_{RM}. In particular, we did not assess whether an infection with the influenza virus would result in a similar phenotype as in vivo activation of HA-specific T cells with the adjuvanted influenza vaccine. Finally, another limitation of our study is that we have not yet addressed to what extent brain-resident CD4 T cells induce the loss of neurons, independently on their role in promoting CD8 T_{RM} maintenance and effector functions. Further investigations will be needed to decipher the relative contribution and the interplay of CD4 T_{RM} and CD8 T_{RM} in the context of chronic CNS inflammation. A better understanding of the mechanisms underpinning the adaptation and survival of T_{RM} within the CNS and of their functional heterogeneity represents therefore important opportunities for future therapies against T cell-mediated neuroinflammatory diseases.

Materials and Methods

Study Design

Our research objective was to assess the contribution of $CD8^+$ T_{RM} in autoimmune destruction of CNS neurons. We studied post-mortem samples from 10 patients suffering from autoimmune diseases directed against neuronal antigens (ethical committee numbers: EK1206/2013-EK1123/2015 and AC-2019-3465-AC-2020-3918). We used transgenic mice expressing a neuron-specific neo self-antigen as well as in vitro or in vivo generated effector $CD8^+$ T cells targeting the model autoantigen. We characterized the CNS-infiltrating autoreactive $CD8^+$ T cells using single-cell transcriptomics, flow cytometry, and histology and uncovered their tissue-resident nature and their heterogeneity. We used antibody-mediated depletion to evaluate the dependency of autoreactive tissue-resident $CD8^+$ T cells on $CD4^+$ T cells and circulating $CD8^+$ T cells. The time-points were prospectively selected. Although no formal power analysis was performed, the number of data points, the number of experimental replicates, and the statistical methods are indicated in figure legends. Animals were randomly assigned to the different treatment groups. A single animal was excluded due to a likely genotyping error (Fig 7 F-I). Counting of surviving neurons was performed either in an automated manner or by an investigator blinded to the treatment group. For further details see Supplementary Materials.

Mice

The (BALB/cJ x C57Bl/6J)F1 Orex-HA mice express hemagglutinin (HA) of an H1N1 influenza virus in orexinergic neurons (*26*). The TCR-transgenic mice (BALB/cJ x C57Bl/6J)F1 CL4-TCR and 6.5-TCR, expressing respectively K^d-restricted $HA_{512\text{-}520}$-specific and I-E^d-restricted $HA_{110\text{-}119}$-specific TCR, have been previously described (*30*). The TCR-transgenic mice express the CD45.1 congenic marker, whereas the recipient mice are CD45.2. Male and female mice (5.5-8 week-old) were included in the experiments. All animal

experiments were performed in the UMS006 animal facility, Toulouse, France, in accordance with the European Union guidelines following approval of the local ethics committee (17-U1043 RL/HN-939).

In vitro T-cell differentiation and adoptive transfer of activated $CD8^+$ T cells

HA-specific $CD8^+$ T cells were isolated from spleen and lymph nodes of CL4-TCR mice by negative selection using the Dynabeads Untouched Mouse CD8 Cells kit (Invitrogen). Purified $CD8^+$ T cells were cultivated with irradiated syngeneic splenocytes at a 1:5 ratio in DMEM Glutamax-medium supplemented with 10% fetal calf serum in the presence of 1µg/ml $HA_{512-520}$-peptide, 1ng/ml IL-2, and 20ng/ml IL-12 (all from R&D Systems). After five days of culture, living cells were collected by Ficoll density separation and 3×10^6 activated $CD8^+$ T cells were adoptively transferred i.v. in Orex-HA or HA-negative littermate control mice. The activated $CD8^+$ T cell suspensions routinely contained >95% of $CD8^+V\beta8^+$ and >70% were IFNγ/TNF producers.

Monoclonal antibody depleting treatments

To deplete $CD8^+$ T cells, an anti-CD8α mAb (clone YTS169.4; Invivo BioXcell) was injected i.p. starting eight days after transfer of activated $CD8^+$ T cells (200µg/mouse), then at day 11 and weekly (100 µg/mouse) until sacrifice. To deplete $CD4^+$ T cells, an anti-CD4 mAb (clone GK1.5; Invivo BioXcell) was injected i.p. four days (200µg/mouse) and one day (100µg/mouse) prior to or eight days after adoptive transfer of activated $CD8^+$ T cells, then weekly (100µg/mouse) until sacrifice. For depletion of both $CD4^+$ and $CD8^+$ T cells, the two above-described protocols were combined.

Isolation and stimulation of hypothalamus-infiltrating mononuclear cells

Mice were deeply anesthetized with ketamine (100mg/kg) and xylazine (10mg/kg) and perfused intracardially. Brains were removed and a hypothalamic block was dissected out, homogenized and digested in HBSS medium with collagenase D (1mg/mL), TLCK (30µg/ml)

and DNase I (20µg/mL), all from Roche® Diagnostics. After digestion the hypothalamic cells were suspended in 30% Percoll (GE Healthcare) and spun at a centrifugation step of 1590g for 30min without brake. Myelin and debris were removed and cell suspensions further used for experiments.

Histopathology

Immunofluorescence assays on human and mouse brains were performed on 5µm thick sections. Antibody concentrations and pre-treatments are listed in **Table S3** and information for staining and cell quantification is provided in Supplementary material.

RNA extraction and high-throughput single-cell RNA sequencing

Thirty days after transfer of activated HA-specific $CD8^+$ T cells, the HA-specific $CD8^+$ T cells ($CD11b^-NK1.1^-CD45.2^+CD8^+TCR\beta^+CD45.1^+$) were isolated by FACS sorting (BD FACSAria Fusion) from the spleen and hypothalami of 13 Orex-HA mice. Immediately after cell sorting, cells were subjected to scRNA-seq processing (10X Genomics, Chromium Single Cell 3' v3 kit) according to the manufacturer's instructions. Sequencing was performed on one flowcell of Illumina NovaSeq 6000 sequencer on 3922 splenic and 1421 hypothalamic $CD45.1^+CD8^+$ T cells.

Statistical analyses

Quantitative data are presented as means ± SEM or percentages. Statistical analyses were performed using GraphPad Prism 9. Student's test, Chi^2 test and one-way or two-way analysis of variance (ANOVA) were performed with the appropriate post hoc tests. For non-normally distributed data (Shapiro-Wilk test, $P<0.05$), the non-parametric Mann-Whitney's and Kruskal-Wallis' tests were used. Only two-sided P values ≤ 0.05 were considered statistically significant and are indicated on the figures as follows: * $P<0.05$, ** $P<0.01$, *** $P<0.001$, **** $P<0.0001$.

Supplementary Materials

Supplementary Materials

Figures S1 – S8

Tables S1 – S3

Datafile S1

References (45-49)

References

1. L. Steinman, Immunology of relapse and remission in multiple sclerosis. *Annual review of immunology* **32**, 257-281 (2014).
2. Y. Cao, B. A. Goods, K. Raddassi, G. T. Nepom, W. W. Kwok, J. C. Love, D. A. Hafler, Functional inflammatory profiles distinguish myelin-reactive T cells from patients with multiple sclerosis. *Science translational medicine* **7**, 287ra274 (2015).
3. S. A. Sagan, R. C. Winger, A. Cruz-Herranz, P. A. Nelson, S. Hagberg, C. N. Miller, C. M. Spencer, P. P. Ho, J. L. Bennett, M. Levy, M. H. Levin, A. S. Verkman, L. Steinman, A. J. Green, M. S. Anderson, R. A. Sobel, S. S. Zamvil, Tolerance checkpoint bypass permits emergence of pathogenic T cells to neuromyelitis optica autoantigen aquaporin-4. *Proceedings of the National Academy of Sciences of the United States of America* **113**, 14781-14786 (2016).
4. J. Dalmau, F. Graus, Antibody-Mediated Encephalitis. *The New England journal of medicine* **378**, 840-851 (2018).
5. R. S. Liblau, A. Vassalli, A. Seifinejad, M. Tafti, Hypocretin (orexin) biology and the pathophysiology of narcolepsy with cataplexy. *The Lancet. Neurology* **14**, 318-328 (2015).
6. D. Sulzer, R. N. Alcalay, F. Garretti, L. Cote, E. Kanter, J. Agin-Liebes, C. Liong, C. McMurtrey, W. H. Hildebrand, X. Mao, V. L. Dawson, T. M. Dawson, C. Oseroff, J. Pham, J. Sidney, M. B. Dillon, C. Carpenter, D. Weiskopf, E. Phillips, S. Mallal, B. Peters, A. Frazier, C. S. Lindestam Arlehamn, A. Sette, T cells from patients with Parkinson's disease recognize α-synuclein peptides. *Nature* **546**, 656-661 (2017).

7. A. Willcox, S. J. Richardson, A. J. Bone, A. K. Foulis, N. G. Morgan, Analysis of islet inflammation in human type 1 diabetes. *Clinical and experimental immunology* **155**, 173-181 (2009).

8. L. Yshii, C. Bost, R. Liblau, Immunological Bases of Paraneoplastic Cerebellar Degeneration and Therapeutic Implications. *Frontiers in immunology* **11**, 991 (2020).

9. R. Kapoor, P. R. Ho, N. Campbell, I. Chang, A. Deykin, F. Forrestal, N. Lucas, B. Yu, D. L. Arnold, M. S. Freedman, M. D. Goldman, H. P. Hartung, E. K. Havrdová, D. Jeffery, A. Miller, F. Sellebjerg, D. Cadavid, D. Mikol, D. Steiner, Effect of natalizumab on disease progression in secondary progressive multiple sclerosis (ASCEND): a phase 3, randomised, double-blind, placebo-controlled trial with an open-label extension. *The Lancet. Neurology* **17**, 405-415 (2018).

10. J. Machado-Santos, E. Saji, A. R. Troscher, M. Paunovic, R. Liblau, G. Gabriely, C. G. Bien, J. Bauer, H. Lassmann, The compartmentalized inflammatory response in the multiple sclerosis brain is composed of tissue-resident CD8+ T lymphocytes and B cells. *Brain*, (2018).

11. C. Baecher-Allan, B. J. Kaskow, H. L. Weiner, Multiple Sclerosis: Mechanisms and Immunotherapy. *Neuron* **97**, 742-768 (2018).

12. J. J. Sabatino, Jr., A. K. Pröbstel, S. S. Zamvil, B cells in autoimmune and neurodegenerative central nervous system diseases. *Nature reviews. Neuroscience* **20**, 728-745 (2019).

13. K. van Gisbergen, K. D. Zens, C. Münz, T-cell memory in tissues. *European journal of immunology* **51**, 1310-1324 (2021).

14. D. Masopust, A. G. Soerens, Tissue-Resident T Cells and Other Resident Leukocytes. *Annual review of immunology* **37**, 521-546 (2019).

15. S. L. Park, L. K. Mackay, Decoding Tissue-Residency: Programming and Potential of Frontline Memory T Cells. *Cold Spring Harbor perspectives in biology* **13**, (2021).

16. K. Steinbach, I. Vincenti, M. Kreutzfeldt, N. Page, A. Muschaweckh, I. Wagner, I. Drexler, D. Pinschewer, T. Korn, D. Merkler, Brain-resident memory T cells represent an autonomous

cytotoxic barrier to viral infection. *The Journal of experimental medicine* **213**, 1571-1587 (2016).

17. J. Smolders, K. M. Heutinck, N. L. Fransen, E. B. M. Remmerswaal, P. Hombrink, I. J. M. Ten Berge, R. A. W. van Lier, I. Huitinga, J. Hamann, Tissue-resident memory T cells populate the human brain. *Nature communications* **9**, 4593 (2018).
18. K. Okła, D. L. Farber, W. Zou, Tissue-resident memory T cells in tumor immunity and immunotherapy. *The Journal of experimental medicine* **218**, (2021).
19. G. E. Ryan, J. E. Harris, J. M. Richmond, Resident Memory T Cells in Autoimmune Skin Diseases. *Frontiers in immunology* **12**, 652191 (2021).
20. B. D. Hondowicz, D. An, J. M. Schenkel, K. S. Kim, H. R. Steach, A. T. Krishnamurty, G. J. Keitany, E. N. Garza, K. A. Fraser, J. J. Moon, W. A. Altemeier, D. Masopust, M. Pepper, Interleukin-2-Dependent Allergen-Specific Tissue-Resident Memory Cells Drive Asthma. *Immunity* **44**, 155-166 (2016).
21. E. Kuric, P. Seiron, L. Krogvold, B. Edwin, T. Buanes, K. F. Hanssen, O. Skog, K. Dahl-Jørgensen, O. Korsgren, Demonstration of Tissue Resident Memory CD8 T Cells in Insulitic Lesions in Adult Patients with Recent-Onset Type 1 Diabetes. *The American journal of pathology* **187**, 581-588 (2017).
22. S. Zundler, E. Becker, M. Spocinska, M. Slawik, L. Parga-Vidal, R. Stark, M. Wiendl, R. Atreya, T. Rath, M. Leppkes, K. Hildner, R. López-Posadas, S. Lukassen, A. B. Ekici, C. Neufert, I. Atreya, K. van Gisbergen, M. F. Neurath, Hobit- and Blimp-1-driven CD4(+) tissue-resident memory T cells control chronic intestinal inflammation. *Nature immunology* **20**, 288-300 (2019).
23. N. L. Fransen, C. C. Hsiao, M. van der Poel, H. J. Engelenburg, K. Verdaasdonk, M. C. J. Vincenten, E. B. M. Remmerswaal, T. Kuhlmann, M. R. J. Mason, J. Hamann, J. Smolders, I. Huitinga, Tissue-resident memory T cells invade the brain parenchyma in multiple sclerosis white matter lesions. *Brain* **143**, 1714-1730 (2020).
24. E. Beltrán, L. A. Gerdes, J. Hansen, A. Flierl-Hecht, S. Krebs, H. Blum, B. Ertl-Wagner, F. Barkhof, T. Kümpfel, R. Hohlfeld, K. Dornmair, Early adaptive immune activation detected in

monozygotic twins with prodromal multiple sclerosis. *The Journal of clinical investigation* **129**, 4758-4768 (2019).

25. C. G. Bien, A. Vincent, M. H. Barnett, A. J. Becker, I. Blümcke, F. Graus, K. A. Jellinger, D. E. Reuss, T. Ribalta, J. Schlegel, I. Sutton, H. Lassmann, J. Bauer, Immunopathology of autoantibody-associated encephalitides: clues for pathogenesis. *Brain* **135**, 1622-1638 (2012).

26. R. Bernard-Valnet, L. Yshii, C. Quériault, X. H. Nguyen, S. Arthaud, M. Rodrigues, A. Canivet, A. L. Morel, A. Matthys, J. Bauer, B. Pignolet, Y. Dauvilliers, C. Peyron, R. S. Liblau, CD8 T cell-mediated killing of orexinergic neurons induces a narcolepsy-like phenotype in mice. *Proceedings of the National Academy of Sciences of the United States of America* **113**, 10956-10961 (2016).

27. L. M. Wakim, A. Woodward-Davis, R. Liu, Y. Hu, J. Villadangos, G. Smyth, M. J. Bevan, The molecular signature of tissue resident memory CD8 T cells isolated from the brain. *J Immunol* **189**, 3462-3471 (2012).

28. I. Uddbäck, E. K. Cartwright, A. S. Schøller, A. N. Wein, S. L. Hayward, J. Lobby, S. Takamura, A. R. Thomsen, J. E. Kohlmeier, J. P. Christensen, Long-term maintenance of lung resident memory T cells is mediated by persistent antigen. *Mucosal immunology* **14**, 92-99 (2021).

29. J. S. Low, Y. Farsakoglu, M. C. Amezcua Vesely, E. Sefik, J. B. Kelly, C. C. D. Harman, R. Jackson, J. A. Shyer, X. Jiang, L. S. Cauley, R. A. Flavell, S. M. Kaech, Tissue-resident memory T cell reactivation by diverse antigen-presenting cells imparts distinct functional responses. *The Journal of experimental medicine* **217**, (2020).

30. R. Bernard-Valnet, D. Frieser, X. H. Nguyen, L. Khajavi, C. Quériault, S. Arthaud, S. Melzi, M. Fusade-Boyer, F. Masson, M. Zytnicki, A. Saoudi, Y. Dauvilliers, C. Peyron, J. Bauer, R. S. Liblau, Influenza vaccination induces autoimmunity against orexinergic neurons in a mouse model for narcolepsy. *Brain* **In Press**, (2022).

31. H. M. Ren, E. M. Kolawole, M. Ren, G. Jin, C. S. Netherby-Winslow, Q. Wade, Shwetank, Z. S. M. Rahman, B. D. Evavold, A. E. Lukacher, IL-21 from high-affinity CD4 T cells drives

differentiation of brain-resident CD8 T cells during persistent viral infection. *Science immunology* **5**, (2020).

32. T. E. Mockus, Shwetank, M. D. Lauver, H. M. Ren, C. S. Netherby, T. Salameh, Y. I. Kawasawa, F. Yue, J. R. Broach, A. E. Lukacher, CD4 T cells control development and maintenance of brain-resident CD8 T cells during polyomavirus infection. *PLoS pathogens* **14**, e1007365 (2018).

33. Y. M. Son, I. S. Cheon, Y. Wu, C. Li, Z. Wang, X. Gao, Y. Chen, Y. Takahashi, Y. X. Fu, A. L. Dent, M. H. Kaplan, J. J. Taylor, W. Cui, J. Sun, Tissue-resident CD4(+) T helper cells assist the development of protective respiratory B and CD8(+) T cell memory responses. *Science immunology* **6**, (2021).

34. B. Engelhardt, P. Vajkoczy, R. O. Weller, The movers and shapers in immune privilege of the CNS. *Nature immunology* **18**, 123-131 (2017).

35. K. Alves de Lima, J. Rustenhoven, J. Kipnis, Meningeal Immunity and Its Function in Maintenance of the Central Nervous System in Health and Disease. *Annual review of immunology* **38**, 597-620 (2020).

36. J. L. Pappalardo, L. Zhang, M. K. Pecsok, K. Perlman, C. Zografou, K. Raddassi, A. Abulaban, S. Krishnaswamy, J. Antel, D. van Dijk, D. A. Hafler, Transcriptomic and clonal characterization of T cells in the human central nervous system. *Science immunology* **5**, (2020).

37. L. M. Wakim, A. Woodward-Davis, M. J. Bevan, Memory T cells persisting within the brain after local infection show functional adaptations to their tissue of residence. *Proceedings of the National Academy of Sciences of the United States of America* **107**, 17872-17879 (2010).

38. N. Page, S. Lemeille, I. Vincenti, B. Klimek, A. Mariotte, I. Wagner, G. Di Liberto, J. Kaye, D. Merkler, Persistence of self-reactive CD8+ T cells in the CNS requires TOX-dependent chromatin remodeling. *Nature communications* **12**, 1009 (2021).

39. J. Galiano-Landeira, A. Torra, M. Vila, J. Bové, CD8 T cell nigral infiltration precedes synucleinopathy in early stages of Parkinson's disease. *Brain* **143**, 3717-3733 (2020).

40. L. Kok, F. E. Dijkgraaf, J. Urbanus, K. Bresser, D. W. Vredevoogd, R. F. Cardoso, L. Perié, J. B. Beltman, T. N. Schumacher, A committed tissue-resident memory T cell precursor within the circulating CD8+ effector T cell pool. *The Journal of experimental medicine* **217**, (2020).

41. A. Palanichamy, S. Jahn, D. Nickles, M. Derstine, A. Abounasr, S. L. Hauser, S. E. Baranzini, D. Leppert, H. C. von Büdingen, Rituximab efficiently depletes increased CD20-expressing T cells in multiple sclerosis patients. *J Immunol* **193**, 580-586 (2014).

42. C. C. Hsiao, N. L. Fransen, A. M. R. van den Bosch, K. I. M. Brandwijk, I. Huitinga, J. Hamann, J. Smolders, White matter lesions in multiple sclerosis are enriched for CD20(dim) CD8(+) tissue-resident memory T cells. *European journal of immunology* **51**, 483-486 (2021).

43. F. Alfei, K. Kanev, M. Hofmann, M. Wu, H. E. Ghoneim, P. Roelli, D. T. Utzschneider, M. von Hoesslin, J. G. Cullen, Y. Fan, V. Eisenberg, D. Wohlleber, K. Steiger, D. Merkler, M. Delorenzi, P. A. Knolle, C. J. Cohen, R. Thimme, B. Youngblood, D. Zehn, TOX reinforces the phenotype and longevity of exhausted T cells in chronic viral infection. *Nature* **571**, 265-269 (2019).

44. J. J. Milner, C. Toma, Z. He, N. S. Kurd, Q. P. Nguyen, B. McDonald, L. Quezada, C. E. Widjaja, D. A. Witherden, J. T. Crowl, L. A. Shaw, G. W. Yeo, J. T. Chang, K. D. Omilusik, A. W. Goldrath, Heterogenous Populations of Tissue-Resident CD8(+) T Cells Are Generated in Response to Infection and Malignancy. *Immunity* **52**, 808-824.e807 (2020).

45. I. Vincenti, N. Page, K. Steinbach, A. Yermanos, S. Lemeille, N. Nunez, M. Kreutzfeld, B. Klimek, G. Di Liberto, K. Egervari, M. Piccinno, G. Shammas, A. Mariotte, N. Fonta, A.R. Liuzzi, I. Wagner, C. Saadi, C. Stadelmann, S. Reddy, B. Becher, D. Merkler, Tissue-resident CD8+ T cells cooperate with CD4+ T cells to drive compartmentalized immunopathology in the CNS. *Science translational medicine* In press.

46. J. H. Levine, E. F. Simonds, S. C. Bendall, K. L. Davis, A. D. Amir el, M. D. Tadmor, O. Litvin, H. G. Fienberg, A. Jager, E. R. Zunder, R. Finck, A. L. Gedman, I. Radtke, J. R.

Downing, D. Pe'er, G. P. Nolan, Data-Driven Phenotypic Dissection of AML Reveals Progenitor-like Cells that Correlate with Prognosis. *Cell* **162**, 184-197 (2015).

47. A. Yermanos, A. Agrafiotis, R. Kuhn, D. Robbiani, J. Yates, C. Papadopoulou, J. Han, I. Sandu, C. Weber, F. Bieberich, R. Vazquez-Lombardi, A. Dounas, D. Neumeier, A. Oxenius, S. T. Reddy, Platypus: an open-access software for integrating lymphocyte single-cell immune repertoires with transcriptomes. *NAR genomics and bioinformatics* **3**, lqab023 (2021).

48. G. Korotkevich, V. Sukhov, N. Budin, B. Shpak, M. N. Artyomov, A. Sergushichev, Fast gene set enrichment analysis. *bioRxiv*, 060012 (2021).

49. T. A. Doering, A. Crawford, J. M. Angelosanto, M. A. Paley, C. G. Ziegler, E. J. Wherry, Network analysis reveals centrally connected genes and pathways involved in CD8+ T cell exhaustion versus memory. *Immunity* **37**, 1130-1144 (2012).

50. S. Mostafavi, H. Yoshida, D. Moodley, H. LeBoité, K. Rothamel, T. Raj, C. J. Ye, N. Chevrier, S. Y. Zhang, T. Feng, M. Lee, J. L. Casanova, J. D. Clark, M. Hegen, J. B. Telliez, N. Hacohen, P. L. De Jager, A. Regev, D. Mathis, C. Benoist, Parsing the Interferon Transcriptional Network and Its Disease Associations. *Cell* **164**, 564-578 (2016).

Acknowledgments

We thank Drs. Abdelhadi Saoudi and Nicolas Blanchard for their insightful comments on the manuscript. We are indebted to the Cytometry platform of Infinity and the UMS06 for mouse handling and histopathology and to Ulrike Köck and Samantha Mila for technical support. We thank Dr. David Meyronet and Centre de Resources Biologiques - Tissus Tumorothèque Est des Hospices Civils de Lyon for human tissue samples.

Funding: This work was supported by grants from

Agence Nationale pour la Recherche CE17-0014 (to RSL), ERA-Net Narcomics (to RSL), ARSEP-French MS society (to RSL),BETPSY RHU 18- RHUS-0012 (to RSL), the Swiss

National Science Foundation 310030B_201271 & 310030_185321 (to DM), ERC 865026 (to DM), and the Austrian Science Fund FWF: P34864-B (to JB).

Author contributions: DF, JB, FM, RSL conceived the study. DF, AP, and CGF performed all the experiments related to the adoptive transfer mouse model. DF and XHN performed all the experiments related to the vaccine-induced mouse model. AP, KMM and DM performed the histological experiments. DF, LK, AY, AP, KMM, DM, RH, VD, JB, FM, RSL analyzed data and provided critical insight or reagents. FM, RSL wrote the first draft of the paper. DF, AP, LK, CGF, DM, JB edited the paper. All authors reviewed and approved the manuscript.

Competing interests: RSL received grant support from GlaxoSmithKline and BMS. He received speaker or scientific board honoraria from Biogen, Merck, Roche, Novartis, and Sanofi-Genzyme. RH reports speaker´s honoraria from Novartis and Biogen. The Medical University of Vienna (employer of Dr. Höftberger) receives payment for antibody assays and for antibody validation experiments organized by Euroimmun (Lübeck, Germany). The other authors declare no competing interests.

Data and materials availability: All data associated with this study are present in the paper or the Supplementary Materials. The RNA-seq data have been deposited in GEO (accession number GSE195600) and ArrayExpress (accession number E-MTAB-11416)

Figures legends

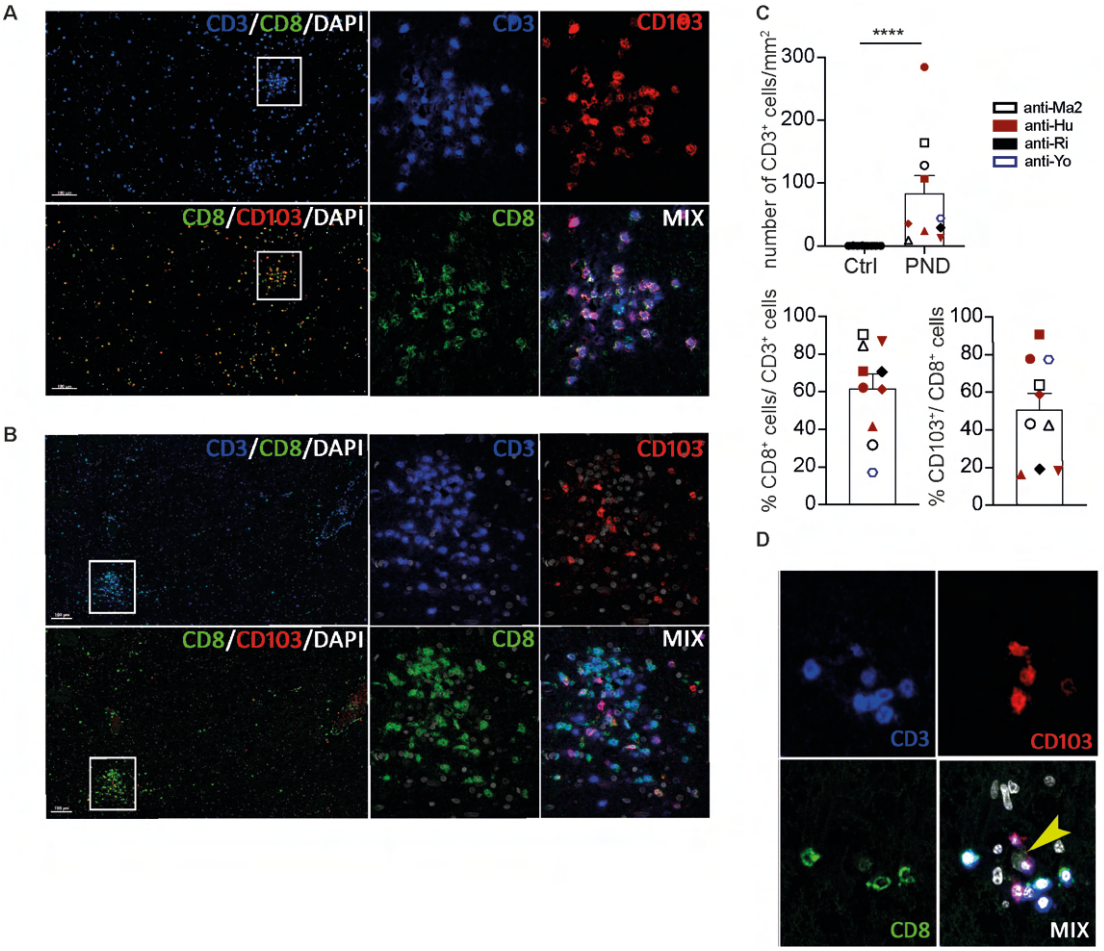

Figure 1. CD8$^+$ T_{RM}-like cells are largely represented within lesions from neuron-targeting autoimmune encephalitis. (A) Representative immunostaining of CD103-expressing CD8$^+$ T_{RM}-like cells within brainstem lesions of anti-Hu antibody-associated paraneoplastic encephalomyelitis, and **(B)** anti-Ri antibody-associated encephalitis. Scale bars: 100 µm. **(C)** Quantification of the density of T cells (left), the proportion of CD8$^+$ cells among T cells (middle) and the frequency of CD103-expressing CD8 T cells (right) in brains, and one dorsal root ganglion, of 10 patients with autoimmune diseases targeting intracellular neuronal self-antigens (5 anti-Hu, 3 anti-Ma2, 1 anti-Yo, and 1 anti-Ri antibody-associated syndromes) and 8 non-neurological controls. Each symbol represents a given patient and the color indicates the antibody-associated syndrome. Statistical analyses were performed using the Mann-Whitney's test. **(D)** Microphotographs documenting close apposition of

$CD3^+CD8^+CD103^+$ and $CD3^+CD8^-CD103^+$ T cells to a neuron (arrow) in the cerebellum of anti-Ma2 antibody-associated encephalitis.

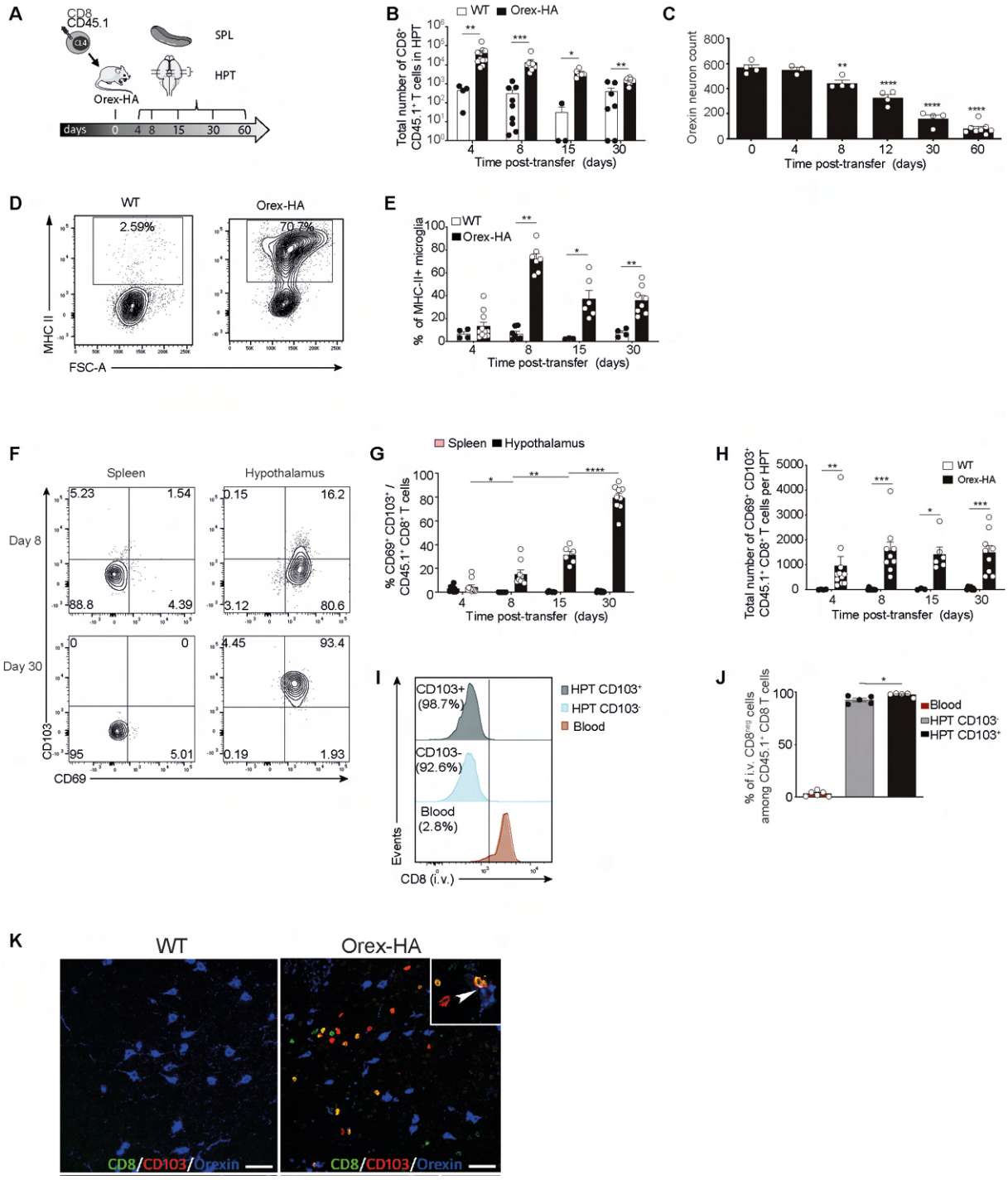

Figure 2. HA-specific CD8$^+$ T cells adopt a tissue-resident phenotype in the hypothalamus, and induce a progressive loss of orexin neurons in Orex-HA mice. (A) Experimental design: Orex-HA mice or wild-type (WT) littermate controls (all CD45.1-negative) were adoptively transferred i.v. with CD45.1$^+$ HA-specific effector CD8$^+$ T cells from CL4-TCR transgenic mice. Spleen (SPL) and hypothalamus (HPT) were analyzed at different time-points post-transfer. **(B)** Numbers of transferred CD8$^+$ T cells (live CD11b$^-$

TCRβ^{+}CD8^{+}CD45.1^{+} cells) in the hypothalamus of Orex-HA and WT mice at different time-points post-transfer in 2 to 5 independent experiments. Each data point (n ranging from 3 to 11) is from 1 to 3 pooled hypothalami. **(C)** Orexin-expressing hypothalamic neurons were quantified by immunohistochemistry in 3 to 8 mice per time-point from 3 independent experiments. **(D)** Representative FACS plots on day 8 post-transfer and **(E)** quantification of MHC-class II expression on microglia (live CD45.2^{int}CD11b^{int}Ly-6c^{-} cells) in the hypothalamus of Orex-HA *vs.* WT mice in 2 (day 4) to 3 (day 8-30) independent experiments. Each data point (n=3 to 11) is from 1 to 3 pooled hypothalami. **(F)** Representative FACS plots and **(G)** proportion of transferred CD8^{+} T cells expressing CD69 and CD103 in the spleen and hypothalamus of Orex-HA mice at different time-points post-transfer. **(H)** Numbers of CD69^{+} CD103^{+} transferred CD8^{+} T cells in the hypothalamus of Orex-HA and WT mice in 2 (day 4), 3 (day 8-15), and 5 (day 30) independent experiments. Each data point (n=3 to 11) is from 1 to 3 pooled hypothalami. **(I)** Representative histograms and **(J)** frequency of transferred CD8^{+} T cells, from hypothalamus or blood, that were not labeled by fluorescent anti-CD8 mAb injected i.v. 5 minutes before sacrifice of Orex-HA mice at day 30 post-transfer, according to their CD103 expression. Data are from 3 independent experiments with 1-3 pooled Orex-HA mice per data point (n=5-6). **(K)** Immunostaining of hypothalami of WT and Orex-HA mice, at day 30. The inset shows a CD103^{+} CD8^{+} T cell in close apposition to an orexin-expressing neuron. Scale bars: 25 μm. Statistical analyses were performed using multiple Mann-Whitney's test with Benjamini-Hochberg correction (B,E,H), one-way ANOVA with Dunnett's or Tukey's post hoc test (C,G), and paired Student t-test (J).

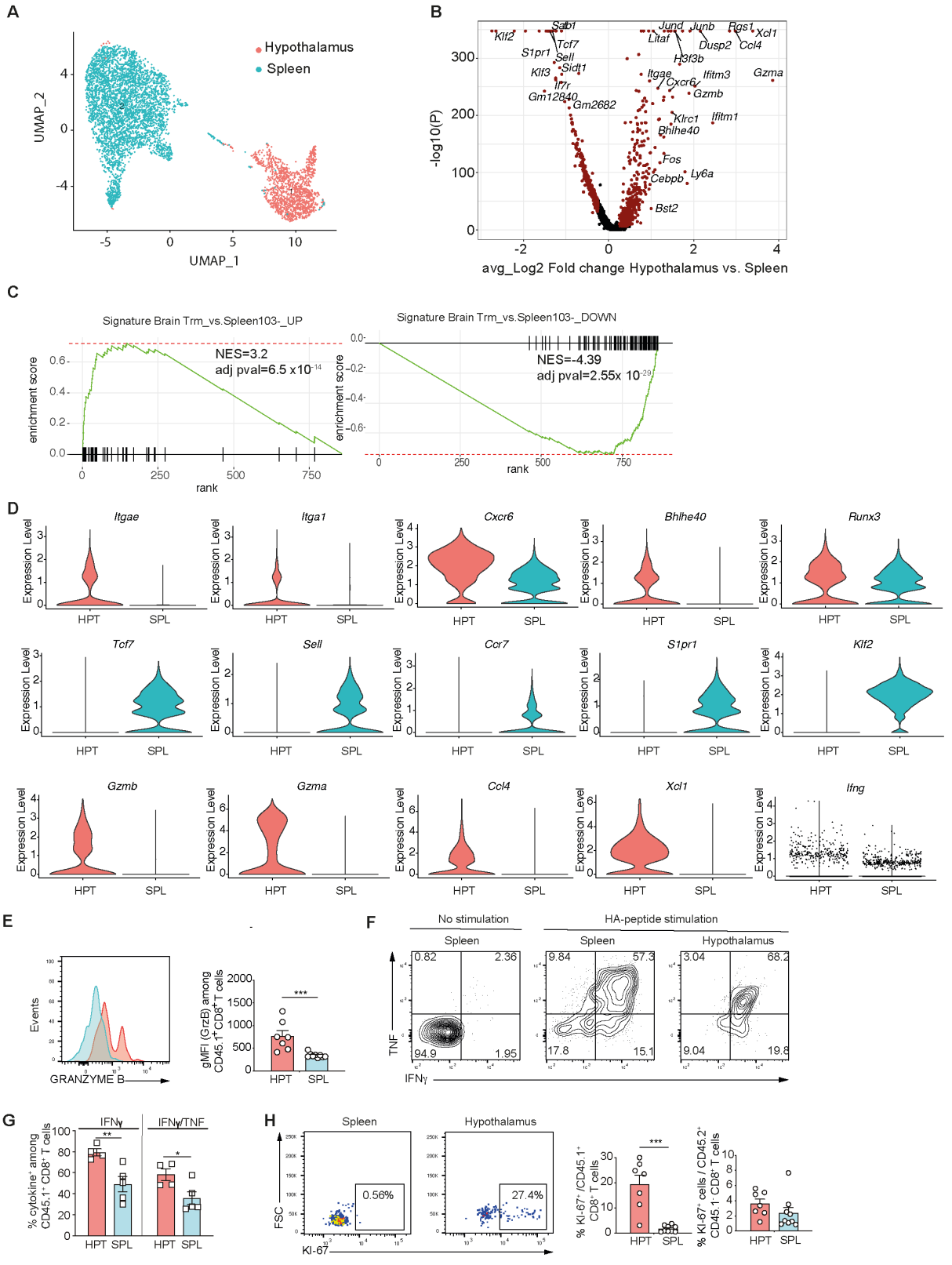

Figure 3. The transcriptional analysis of autoreactive CD8$^+$ T cells from the hypothalamus of Orex-HA mice reveals their T_{RM} identity. (A) UMAP-representation of the single-cell RNA-sequencing dataset from transferred HA-specific CD8$^+$ T cells from the

spleen (blue) and hypothalamus (red) of 13 pooled Orex-HA mice, on day 30. **(B)** Volcano plot of the differentially expressed genes between the hypothalamus and spleen, according to their adjusted P-value and log2-fold change (Log2FC). **(C)** Gene set enrichment analysis (GSEA) of a published brain T_{RM} signature in a ranked list of genes differentially expressed between hypothalamic compared to splenic transferred $CD8^+$ T cells of Orex-HA mice. **(D)** Violin plots of highly up- or down-regulated genes in HA-specific $CD8^+$ T cells from hypothalamus (HPT) *vs.* spleen (SPL). **(E)** Representative histogram and quantification of GRANZYME B expression (gMFI) among splenic and hypothalamic transferred $CD8^+$ T cells from Orex-HA mice, on day 30, in 3 independent experiments. Each data point (n=7-9) involves 2-6 pooled mice. **(F)** Representative FACS plots and **(G)** frequency of TNF/IFNγ expression in splenic and hypothalamic transferred $CD8^+$ T cells from Orex-HA mice on day 30, 6 hrs after ex vivo stimulation with the $HA_{512-520}$ peptide in two independent experiments. Each data point (n=4-5) is from 3-6 pooled mice. **(H)** Representative FACS plots and frequency of Ki-67-expressing splenic and hypothalamic transferred or host $CD8^+$ T cells on day 30 in 3 independent experiments. Each data point (n=7-9) is from 2-6 pooled Orex-HA mice. Statistical analyses were performed using Mann-Whitney test (E,H) and two-way ANOVA with Sidak's post hoc test (G).

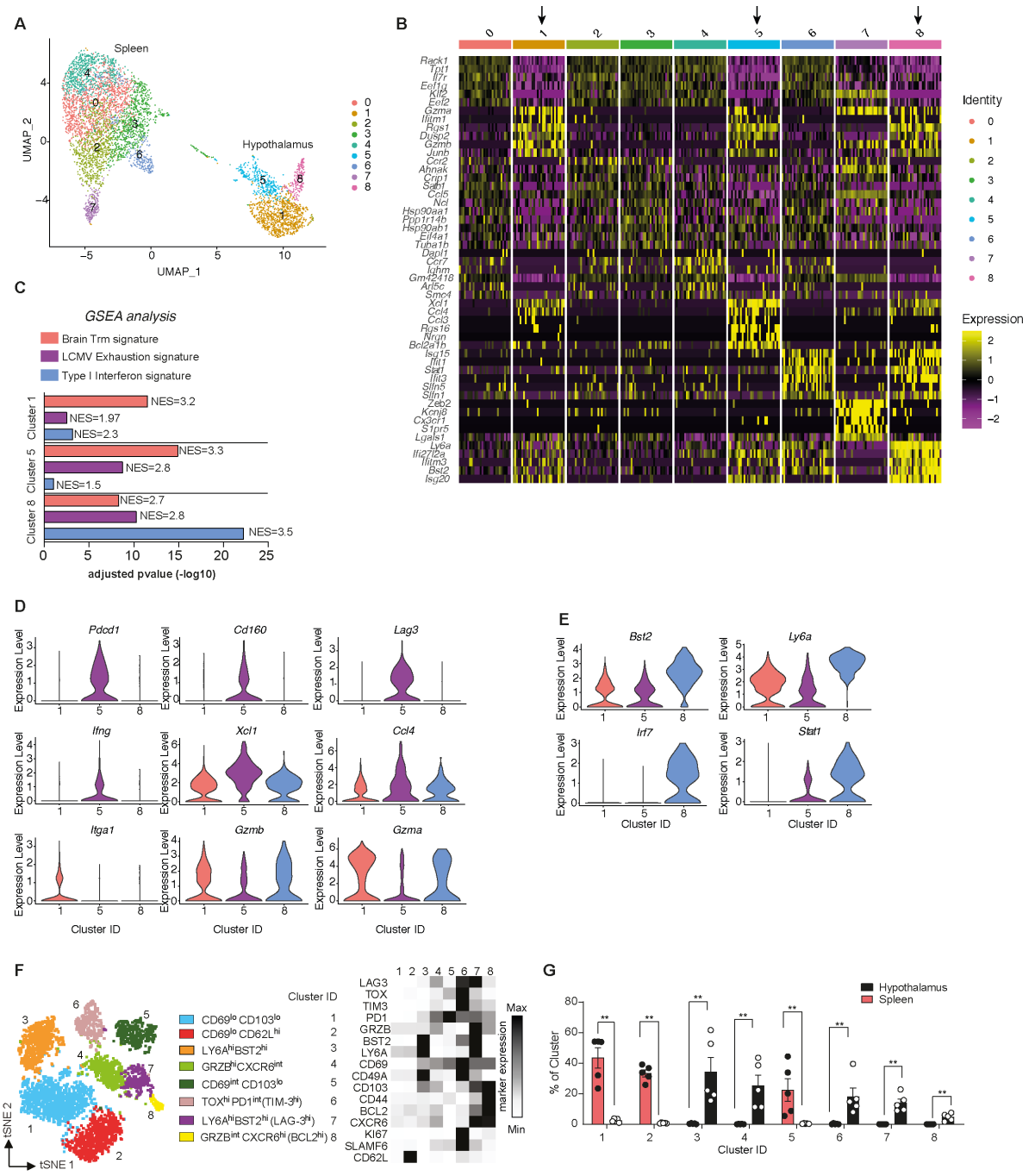

Figure 4. Heterogeneity of autoreactive tissue-resident CD8$^+$ T cells in the hypothalamus

(A) UMAP-representation of SEURAT-generated clusters based on the scRNA-sequencing of splenic and hypothalamic transferred CD8$^+$ T cells from Orex-HA mice, on day 30. **(B)** Heatmap of the five most highly expressed genes in the 9 respective clusters. Arrows indicate the 3 hypothalamic clusters. **(C)** Bar graphs show the adjusted P-value and numeric enrichment score (NES) for the indicated published gene signatures in the transcriptome of the 3 hypothalamic CD8$^+$ T-cell clusters. **(D)** Violin plots of the expression of selected genes

from the effector and exhaustion signatures, and **(E)** type 1 interferon signature in the 3 hypothalamic tissue-resident $CD8^+$ T-cell clusters. **(F)** tSNE-graph of the high-dimensional flow cytometry data, gated on transferred $CD8^+$ T cells from spleen and hypothalamus of Orex-HA mice on day 30 post-transfer, with the cluster overlay (Phenograph) (left) and heatmap of marker expression values (gMFI) in the 8 identified clusters. **(G)** Frequency of the clusters in spleen and hypothalamus of 5 Orex-HA mice from one experiment, representative of 2. Statistical analyses were performed using multiple Mann-Whitney test with Benjamini-Hochberg correction.

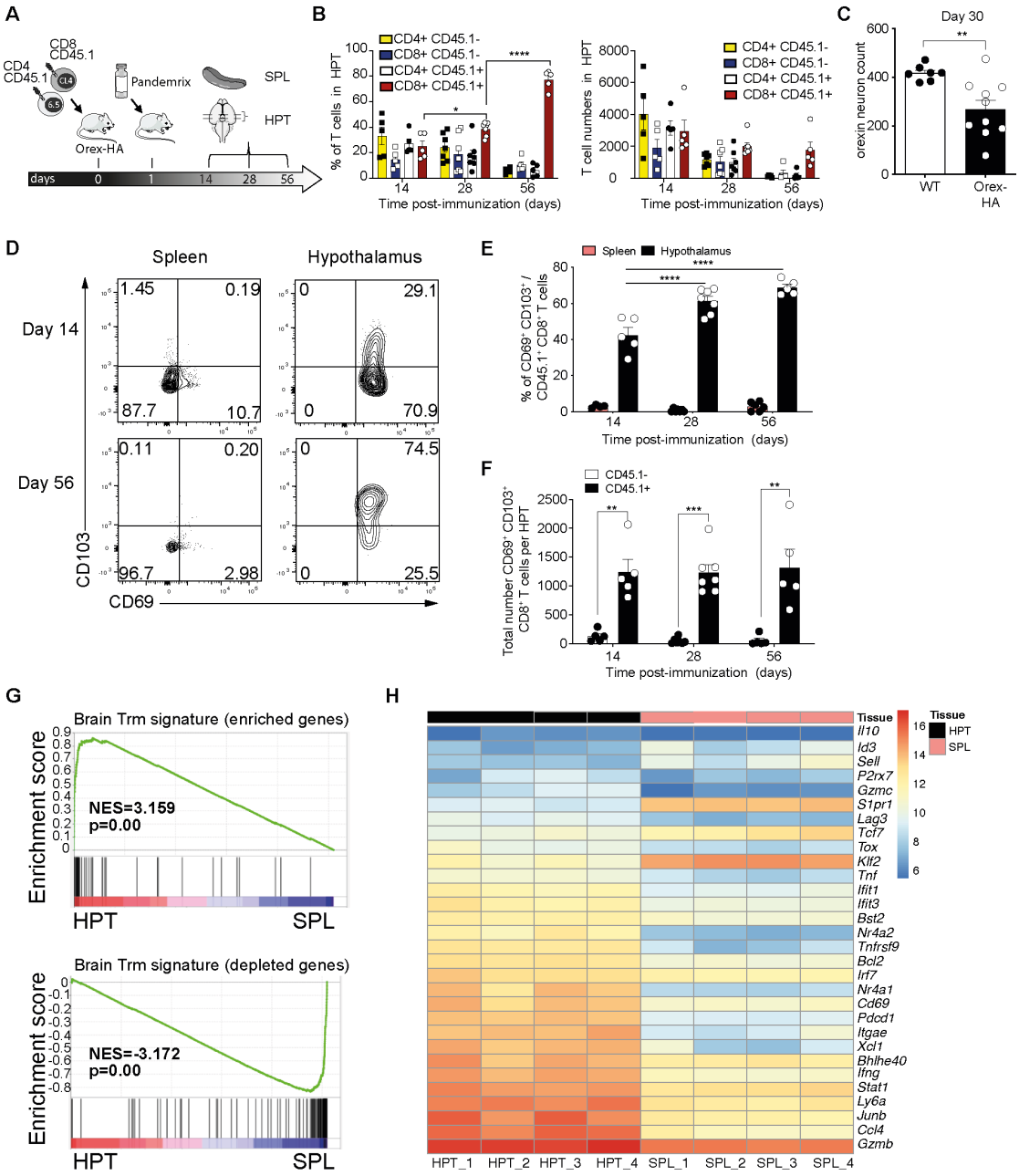

Figure 5. Autoreactive tissue-resident CD8$^+$ T cells arise in the hypothalamus after in vivo priming. (A) Experimental design: Orex-HA or WT mice were adoptively transferred with CD45.1$^+$ naïve HA-specific CD4$^+$ and CD8$^+$ T cells, and vaccinated 24 hrs later with the Pandemrix flu vaccine. **(B)** Absolute numbers of T cells and proportion of CD45.1$^-$ (yellow) and CD45.1$^+$ (green) CD4$^+$ T cells, and of CD45.1$^-$ (blue) and CD45.1$^+$ (red) CD8$^+$ T cells in

the hypothalamus of Orex-HA mice, at different time-points post-vaccination. Graphs show the mean of 5 to 7 data-points (12 to 39 mice) per time-point from 2 to 3 independent experiments. **(C)** Orexin-expressing hypothalamic neurons were quantified by immunohistochemistry 30 days after vaccination in Orex-HA (n=10) and control (n=7) mice from 2 experiments. **(D)** Representative FACS plots and **(E)** frequency of CD69- and CD103-expressing splenic and hypothalamic transferred $CD8^+$ T cells (live $CD11b^-$ $TCR\beta^+CD8^+CD45.1^+$ cells) from Orex-HA mice, at different time-points post-vaccination. **(F)** Absolute numbers of hypothalamic $CD69^+$ $CD103^+$ $CD8^+$ T cells of either endogenous ($CD45.1^-$) or transferred ($CD45.1^+$) origin in Orex-HA mice. Each data point (n=5-7) is from 2-18 pooled hypothalami, and results are from 2 (day 56) to 3 (days 14 and 28) independent experiments. **(G)** GSEA of a published brain T_{RM} signature in a ranked list of genes differentially expressed between hypothalamic *vs.* splenic transferred $CD8^+$ T cells from Orex-HA mice. **(H)** Heatmap of the expression of selected genes in transferred $CD8^+$ T cells from hypothalamus (black) and spleen (red). Statistical analyses were performed using the Mann-Whitney (C), two-way ANOVA with Tukey's (B) or Sidak's post hoc test (E) and multiple Mann-Whitney test with Benjamini-Hochberg correction (F).

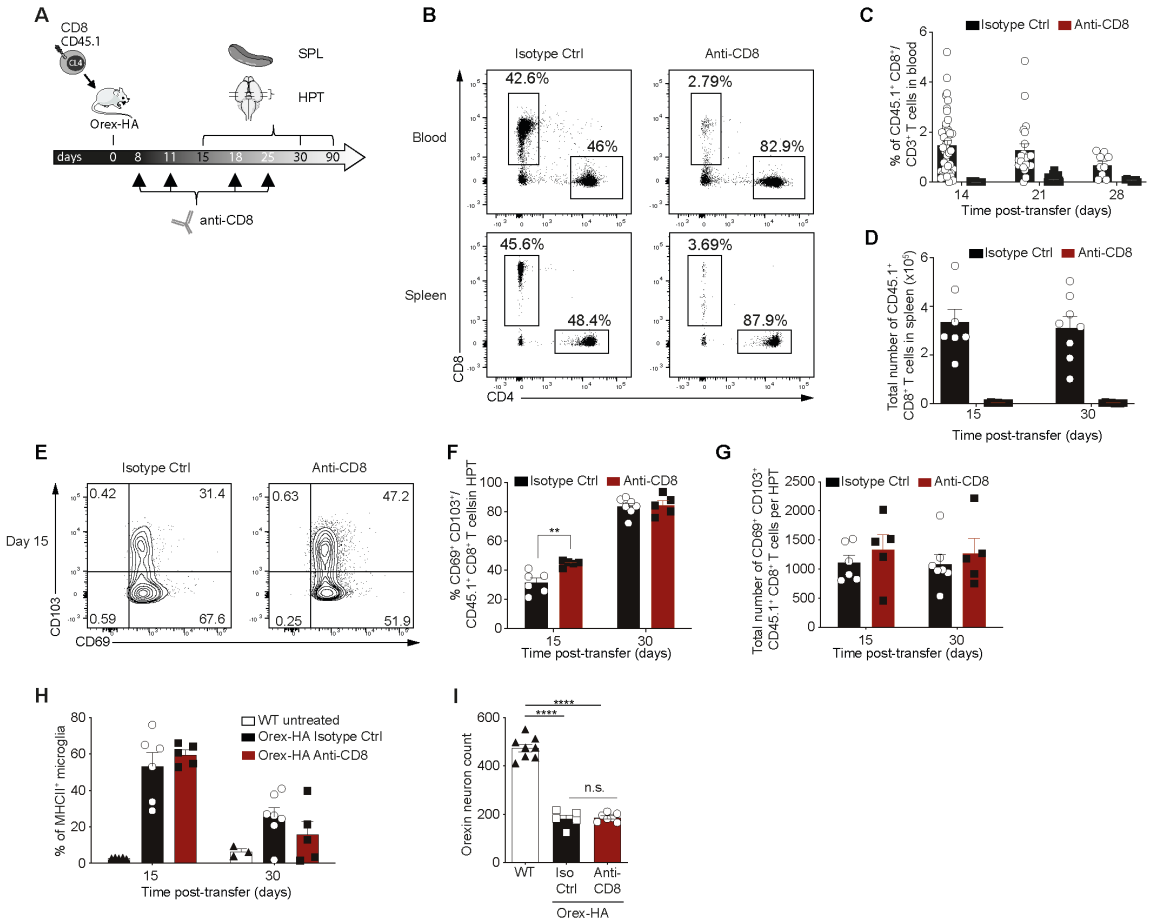

Figure 6. Loss of hypothalamic orexinergic neurons is not dependent on circulating CD8$^+$ T cells. (A) Experimental design: Orex-HA mice were transferred with activated HA-specific CD8$^+$ T cells, and injected with depleting anti-CD8 mAb or isotype control antibodies and sacrificed at the indicated time-points. **(B)** Representative FACS plots of CD4/CD8 staining on live TCRβ$^+$ cells from the blood (top) and spleen (bottom) of Orex-HA mice one week after injection of depleting anti-CD8 mAb or control antibodies. **(C)** Frequency of transferred (CD45.1$^+$CD8$^+$) cells among blood T cells at different time-points (n ranging from 9 mice at day 28 to 43 at day 14). **(D)** Absolute numbers of transferred CD45.1$^+$TCRβ$^+$CD8$^+$ T cells in the spleen of Orex-HA mice treated with depleting anti-CD8 mAb or control antibodies (n=7-8/group per time-point). **(E)** Representative FACS plots on day 15, **(F)** frequency, **(G)** absolute numbers of CD69$^+$ CD103$^+$ transferred CD8$^+$ T cells, and **(H)** MHC-II expression on microglia (live CD45.2^{int}CD11b^{int}Ly-6c$^-$ cells) in the

hypothalamus of Orexin-HA mice treated with anti-CD8 or control antibodies. Each data point (n=5-7) is from 2-pooled mice. Results are from 2 independent experiments per time-point. **(I)** Immunohistochemistry quantification of orexin-expressing hypothalamic neurons at day 30, in 5-8 mice per group from 2 independent experiments. Statistical analyses were performed using two-way ANOVA with Sidak's post hoc test (F-H) and one-way ANOVA with Tukey's post hoc test (I).

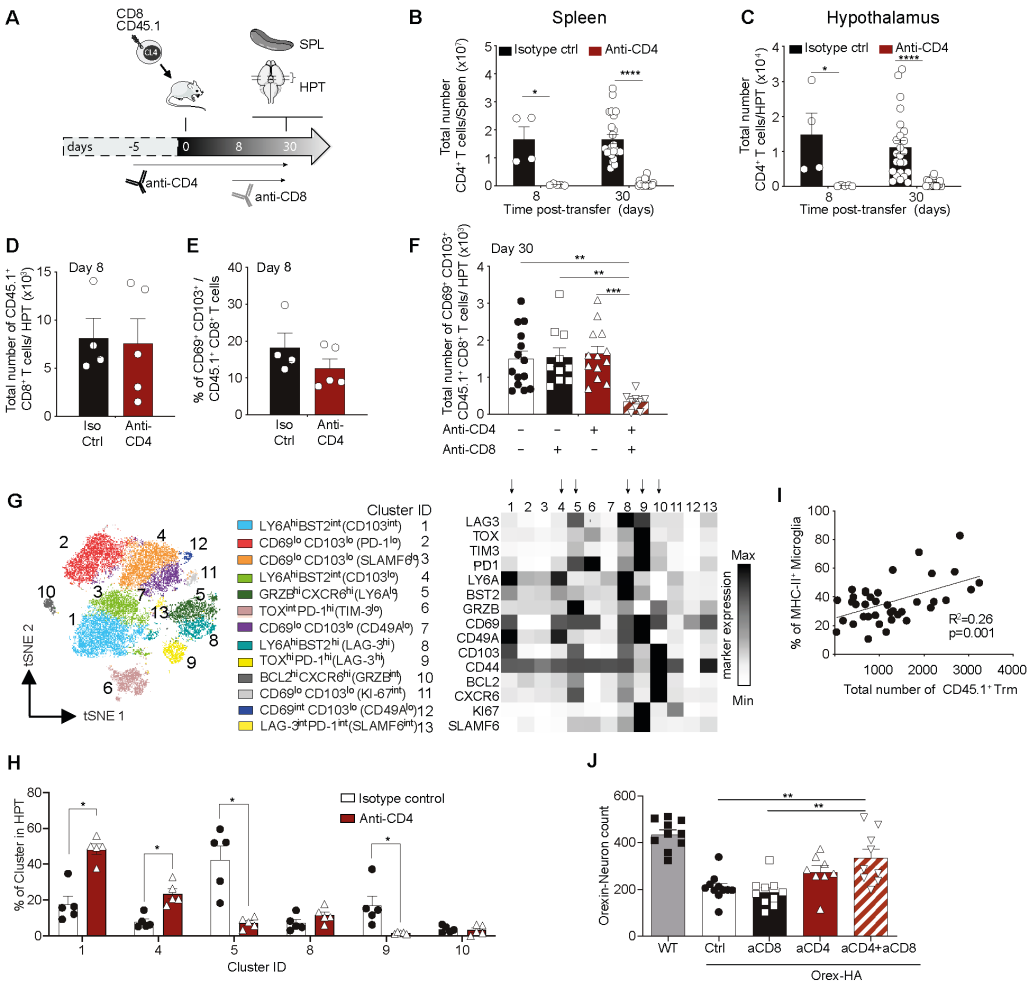

Figure 7. Tissue-resident CD8$^+$ T-cell persistence and their functional properties in the hypothalamus are dependent on CD4$^+$ T cells and are required for sustained neuronal loss. (A) Experimental design: Orex-HA mice were treated with depleting anti-CD4 mAb (or control antibodies) starting 5 days prior to HA-specific CD8$^+$ T-cell transfer. From day 8 onwards, groups of mice also received depleting anti-CD8 mAb (or control antibodies) until sacrifice. **(B)** Absolute numbers of CD4$^+$ T cells in the spleen and **(C)** hypothalamus in Orex-HA mice treated with anti-CD4 mAb or control IgG2b, at different time-points after CD8$^+$ T-cell transfer. The data points are from 2 (day 8; n=4-5 mice/group) or 3 (day 30; n=19-24 mice/group) independent experiments. **(D)** Number of transferred CD8$^+$ T cells and **(E)**

frequency of $CD69^+CD103^+$ among them in the hypothalamus of Orex-HA mice treated with anti-CD4 or isotype control antibodies, on day 8, in 4 to 5 mice per group from 2 independent experiments. **(F)** Numbers of $CD69^+CD103^+$ transferred $CD8^+$ T cells in the hypothalamus of Orex-HA mice treated with control antibodies, with anti-CD8 and/or anti-CD4 mAb, on day 30. Data are from 9 to 14 mice per group in 3 independent experiments. **(G)** tSNE-graph with the cluster overlay (left) of transferred $CD8^+$ T cells from the hypothalamus of the four treatment groups and from the spleen of the IgG2b group, on day 30 post-transfer and heatmap of the expression of key markers (right) in the 13 identified clusters. Arrows indicate the main hypothalamic clusters. **(H)** Frequency of the main hypothalamic clusters in 5 mice per group from one experiment, representative of 2. **(I)** Correlation, on day 30, between MHC-II expression on microglia and the number of $CD69^+CD103^+$ transferred $CD8^+$ T cells in the hypothalamus of Orex-HA mice. The correlation using Pearson's test involves 38 mice from the 4 treatment groups in 3 independent experiments. **(J)** Immunohistochemistry quantification at day 30 of hypothalamic orexin-expressing neurons in 8 to 11 mice per group from 3 independent experiments. Statistical analyses were performed using multiple Mann-Whitney' test with Benjamini-Hochberg correction (B,C,H), Kruskal-Wallis' test with Dunn's post hoc test (F) and one-way ANOVA with Tukey's post hoc test (J).

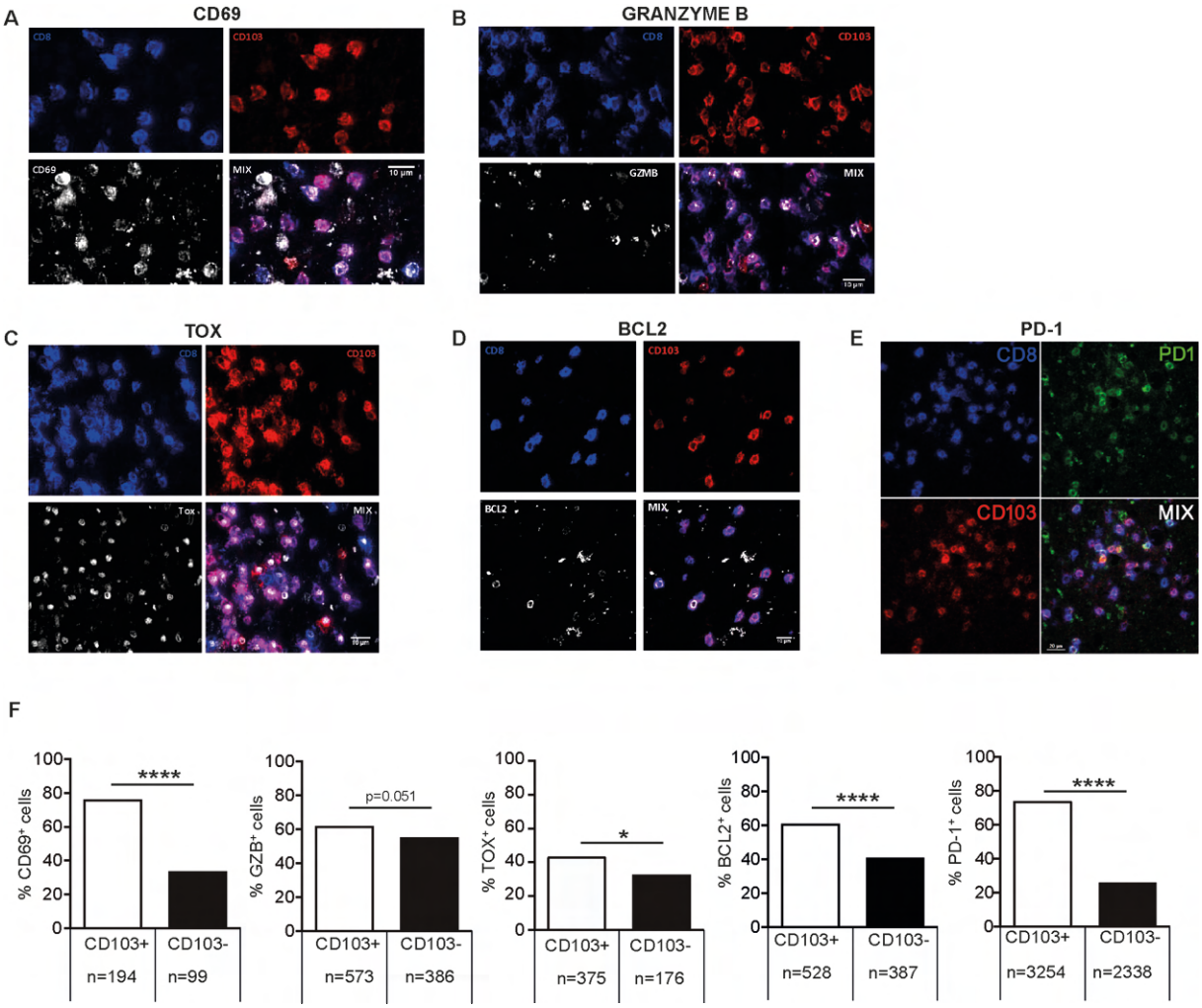

Figure 8. Expression of CD69, GRANZYME B, TOX, BCL-2, and PD-1 in T_{RM}-like $CD8^+$ T cells infiltrating the parenchyma in human neuron-targeting autoimmune encephalitis.

Microphotographs of CNS-infiltrating $CD8^+$ T cells either $CD103^+$ or $CD103^-$, illustrating the expression of CD69 **(A)**, GRANZYME B **(B)**, TOX **(C)**, BCL-2 **(D)** and PD-1 **(E)**. Scale bars: 10 µm in (A-D), and 20 µm in (E). **(F)** Histograms showing the percentage of $CD103^+$ and $CD103^-$ $CD8^+$ T cells expressing CD69 (2 patients, 293 cells), GRANZYME B (9 patients, 959 cells), TOX (4 patients, 551 cells), BCL-2 (9 patients, 915 cells) and PD-1 (6 patients, 5592 cells). Statistical analyses were performed using Chi^2 test with Yates continuity correction.

Supplementary Figures:

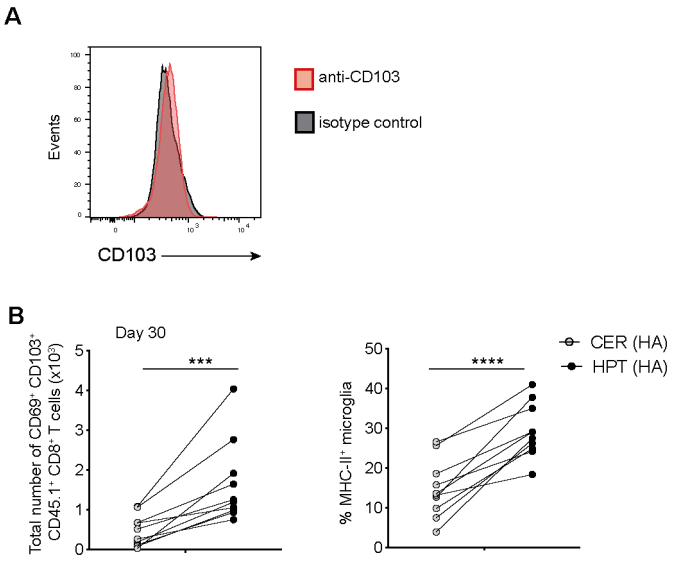

Figure S1. Transferred CD8$^+$ T cells with a tissue-resident phenotype are preferentially located in the hypothalamus of Orex-HA mice. (A) Activated HA-specific CD8$^+$ T cells were analyzed prior to their adoptive transfer for the expression of CD103 expression. One experiment, representative of 9, is shown. **(B)** Number of CD69$^+$CD103$^+$ transferred CD8$^+$ T cells (left) and frequency of MHC-II-expressing microglia (right) in the hypothalamus (black) and cerebellum (grey) of Orex-HA, on day 30 post-transfer. Each data point (n=10) is from 1 to 3 pooled Orex-HA mice. The results are from 3 independent experiments and were analyzed using the paired Student t-test.

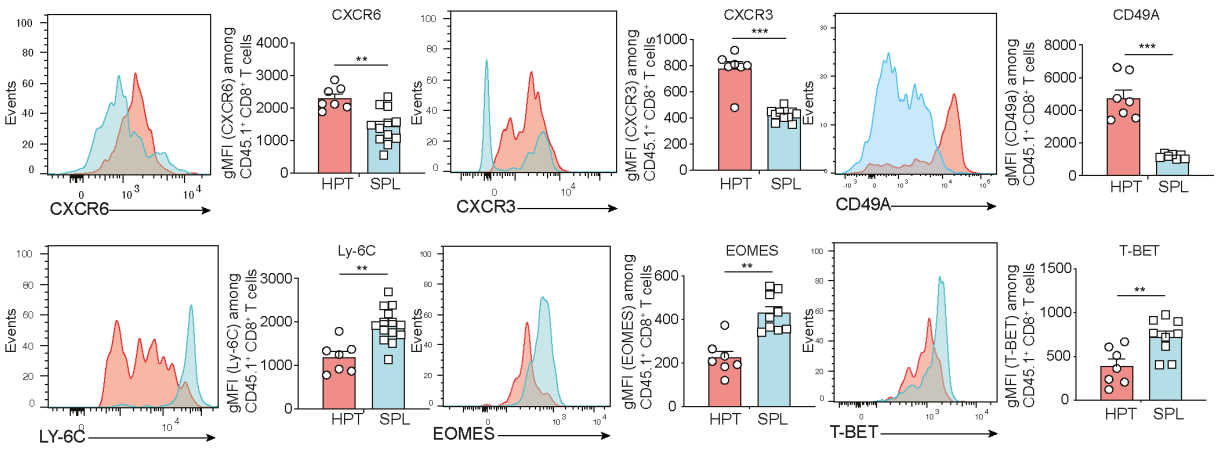

Figure S2. Flow cytometry analyses of autoreactive CD8$^+$ T cells from the hypothalamus of Orex-HA mice confirm their tissue-resident phenotype.

Representative histograms and the quantification of the geometric mean fluorescent intensity (gMFI) of CXCR6, CXCR3, CD49a, Ly-6C, EOMES and T-BET in transferred CD8$^+$ T cells from the spleen and hypothalamus of Orex-HA mice. Each data point (n=7-14) is from 2 to 14 pooled Orex-HA mice. The results are from 3 to 4 independent experiments and were analyzed using the Mann-Whitney's test.

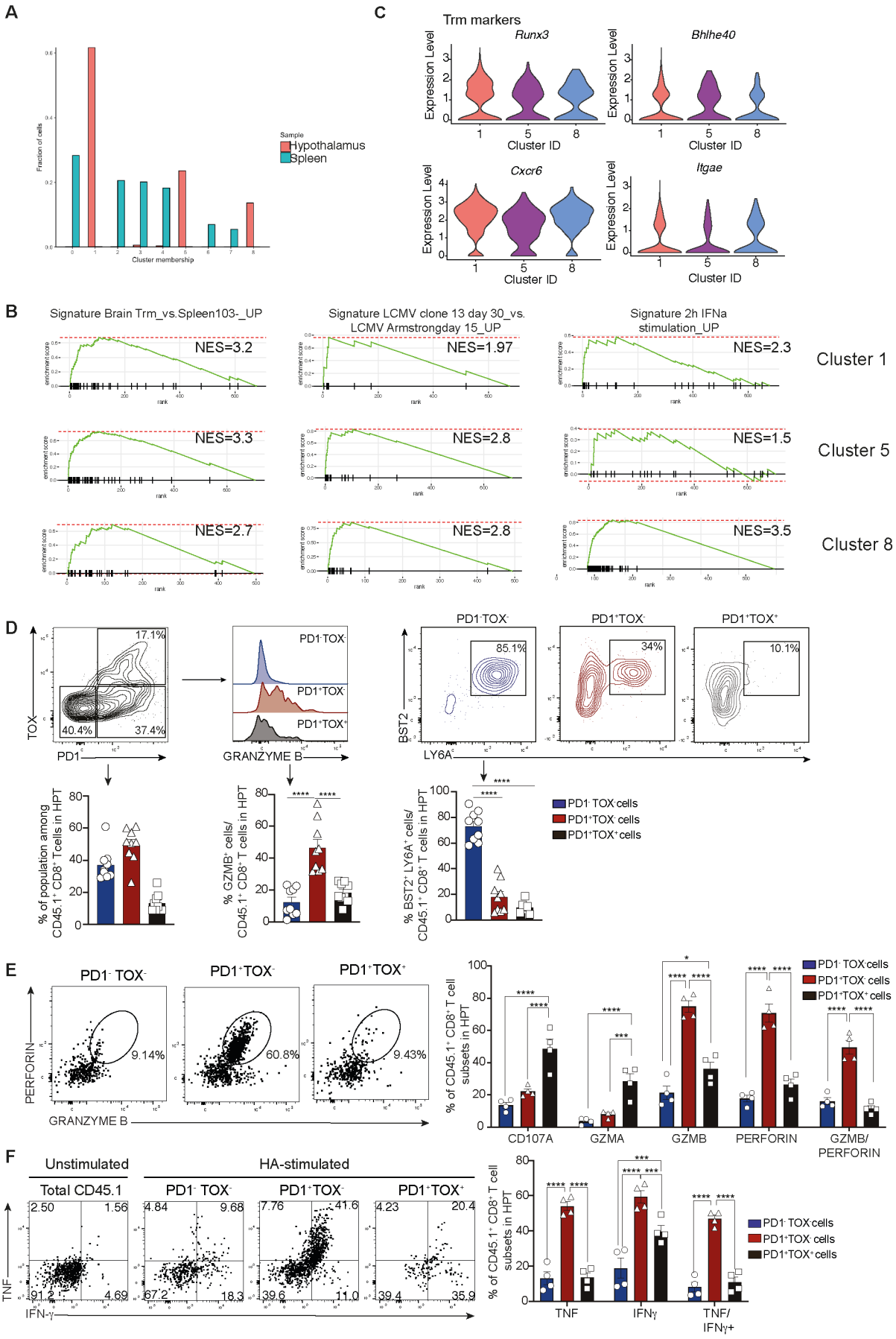
A
Fraction of cells
Cluster membership
Sample
Hypothalamus
Spleen
C
Trm markers
Runx3
Bhlhe40
Cxcr6
Itgae
Expression Level
Cluster ID
B
Signature Brain Trm_vs.Spleen103-_UP
Signature LCMV clone 13 day 30_vs. LCMV Armstrongday 15_UP
Signature 2h IFNa stimulation_UP
NES=3.2
NES=1.97
NES=2.3
NES=3.3
NES=2.8
NES=1.5
NES=2.7
NES=2.8
NES=3.5
Cluster 1
Cluster 5
Cluster 8
enrichment score
rank
D
TOX
PD1
17.1%
40.4%
37.4%
PD1-TOX-
PD1+TOX-
PD1+TOX+
GRANZYME B
BST2
LY6A
85.1%
34%
10.1%
% of population among CD45.1+ CD8+ Tcells in HPT
% GZMB+ cells/ CD45.1+ CD8+ T cells in HPT
% BST2+ LY6A+ cells/ CD45.1+ CD8+ T cells in HPT
PD1- TOX- cells
PD1+TOX- cells
PD1+TOX+ cells
E
PERFORIN
9.14%
60.8%
9.43%
% of CD45.1+ CD8+ T cell subsets in HPT
CD107A
GZMA
GZMB
PERFORIN
GZMB/ PERFORIN
F
Unstimulated
HA-stimulated
Total CD45.1
2.50
1.56
91.2
4.69
4.84
9.68
67.2
18.3
7.76
41.6
39.6
11.0
4.23
20.4
39.4
35.9
TNF
IFN-γ
TNF
IFNγ
TNF/ IFNγ+

Figure S3. Heterogeneity of autoreactive tissue-resident CD8$^+$ T cells in the hypothalamus

(A) Distribution of CD8$^+$ T cells from spleen and hypothalamus of Orex-HA mice in the nine clusters defined by scRNA-sequencing. **(B)** Plots of the GSEA for the brain TRM-, exhaustion- and IFN-signaling signatures in the transcriptome of the three hypothalamic clusters. **(C)** Violin plots showing expression of key brain TRM-signature genes in the 3 hypothalamic clusters. **(D)** Representative FACS plot (top) and quantification (bottom) of PD-1/TOX expression among transferred CD8$^+$ T cells from the hypothalamus of control IgG2b-treated Orex-HA mice, on day 30 (left). GRANZYME B (middle) and BST2 and Ly-6a (right) expression in the three transferred CD8$^+$ T cell populations identified based on PD-1 and TOX expression. Data are from 2 independent experiments involving 9 Orex-HA mice and were analyzed using a one-way ANOVA with Tukey's post hoc test. **(E)** Representative FACS plots (left) of GRANZYME B/PERFORIN co-expression within the three hypothalamic CD45.1$^+$ CD8$^+$ T cell populations of Orex-HA mice, on day 30 after activated CD8$^+$ T cell transfer. Frequency (right) of cells within the 3 hypothalamic CD45.1$^+$ CD8$^+$ T cell subsets expressing CD107a, GRANZYME A (GZMA), GRANZYME B (GZMB), PERFORIN, and GRANZYME B/ PERFORIN. **(F)** Representative FACS plots (*left*) of TNF/IFNγ co-expression within the 3 hypothalamic CD45.1$^+$ CD8$^+$ T cell subsets of Orex-HA mice, on day 30 after activated CD8$^+$ T cell transfer. Frequency (right) of cells within the 3 hypothalamic CD45.1$^+$ CD8$^+$ T cell subsets expressing TNF, IFNγ, and TNF/IFNγ. Each data point (n=4) is from 2 pooled Orex-HA mice and results from one experiment. Statistical analyses in E and F were performed using two-way ANOVA with Tukey's post hoc test.

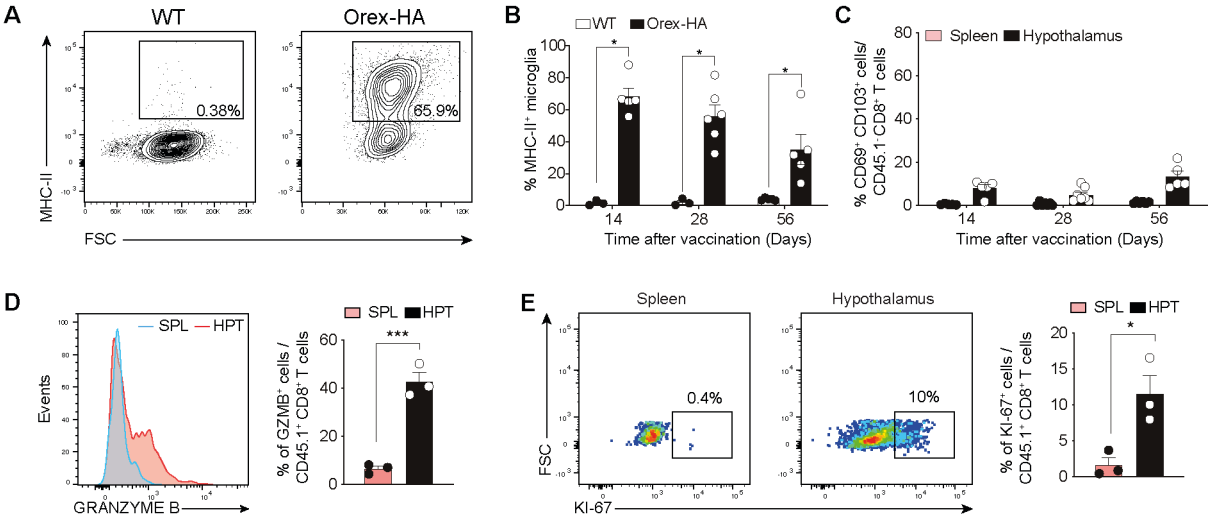

Figure S4. Autoreactive tissue-resident CD8$^+$ T cells arise in the hypothalamus after in vivo priming. (A) Representative histograms and **(B)** frequency of MHC-II expression on microglia (gated on live CD45.2^{int}CD11b^{int}LY-6c$^-$ cells) in the hypothalamus of Orex-HA and littermate control mice. Each data point (n=3-6) is from 2-18 pooled hypothalami and data are from 2 (day 56) or 3 (days 14 and 28) independent experiments. **(C)** Proportion of endogenous (CD45.1$^-$) CD8$^+$ T cells expressing CD69 and CD103 in the spleen and hypothalamus of Orex-HA mice at different time-points post-vaccination. **(D)** Representative histograms and frequency of GRANZYME B-expressing transferred CD8$^+$ T cells in the spleen and hypothalamus of Orex-HA mice on day 28. **(E)** Representative FACS plots and frequency of KI-67-expressing transferred CD8$^+$ T cells in the spleen and hypothalamus on day 28 in one experiment involving 5-6 pooled Orex-HA mice per data point (n=3). Statistical analyses were performed with multiple Mann-Whitney test with Benjamini-Hochberg correction (B) and Student t-test (D,E).

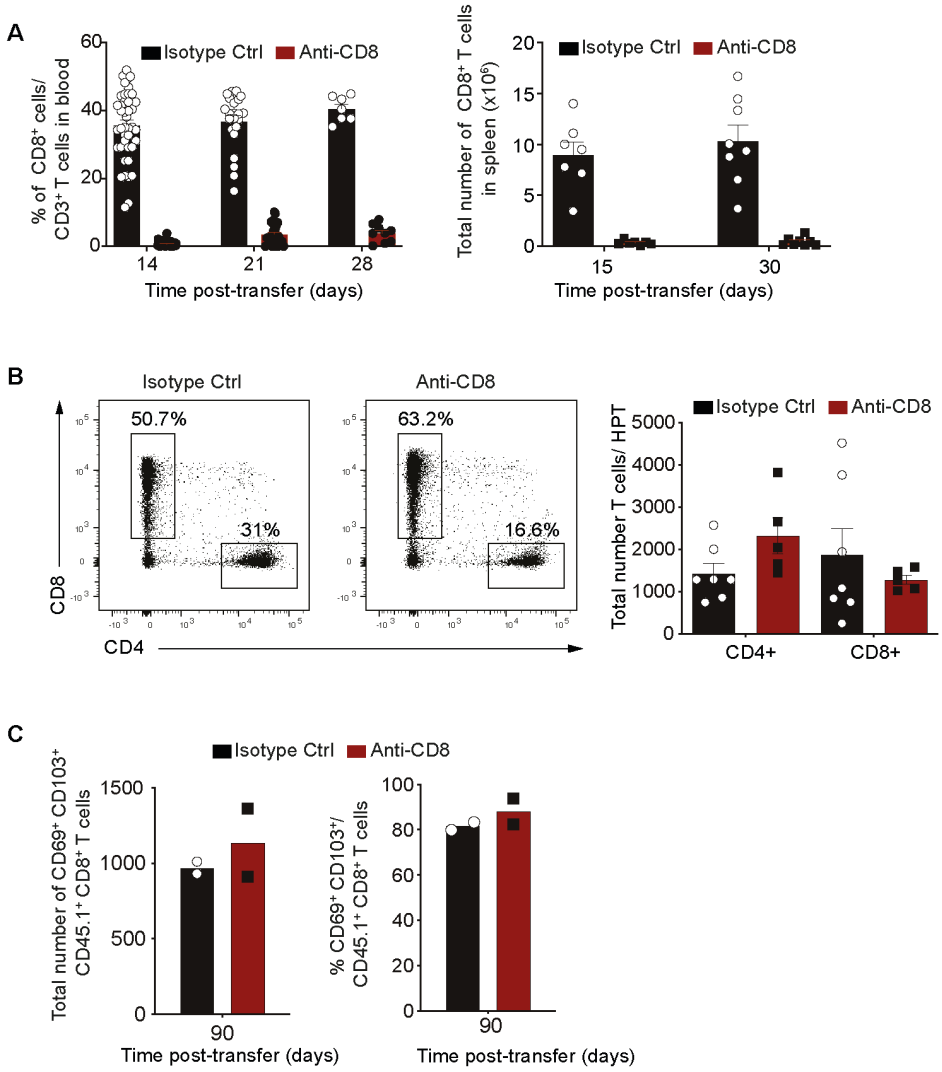

Figure S5. Loss of hypothalamic orexinergic neurons is not dependent on circulating CD8$^+$ T cells. (A) Frequency of blood T cells expressing CD8 (left) and numbers of endogenous (CD45.1$^-$) CD8$^+$ T cells in the spleen (right), at different time-points after injection of anti-CD8 or isotype control antibodies in 2 to 3 independent experiments. Blood: data points represent individual mice (n ranging from 7 at day 28 to 43 at day 14). Spleen: D15: 7 mice per group; D30: 8 mice per group. **(B)** Representative dot-plots and absolute numbers of endogenous T cells in the hypothalamus of Orex-HA mice treated with either anti-CD8 or control antibodies, on day 30. Each data point (n=5-7) is from 2-pooled hypothalami and the data originate from 2 independent experiments. **(C)** Absolute numbers (left) and

frequency (right) of CD69$^+$ CD103$^+$ transferred CD8$^+$ T cells on day 90 in the hypothalamus of Orex-HA mice treated with anti-CD8 or control antibody. Each data point (n= 2) is from 2-pooled mice in one experiment.

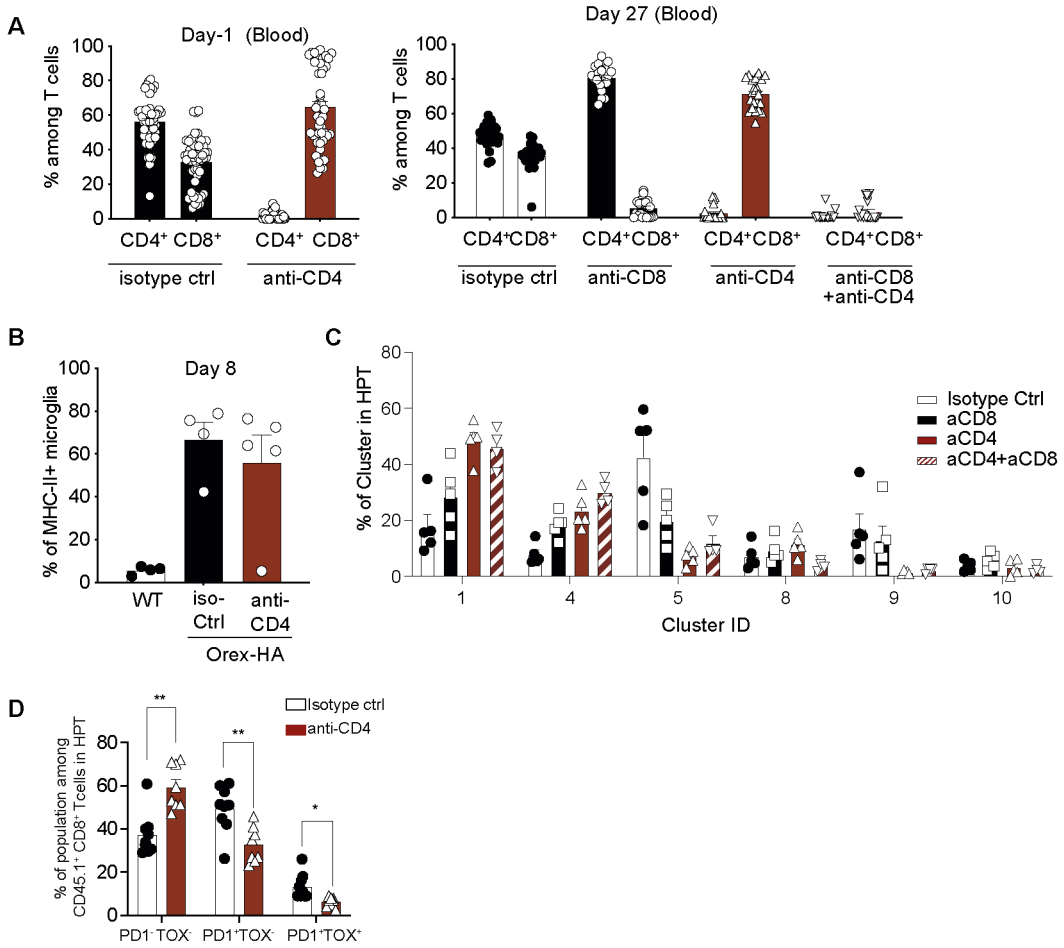

Figure S6. Tissue-resident CD8$^+$ T cell persistence and their functional properties in the hypothalamus are dependent on CD4$^+$ T cells and are required for sustained neuronal loss. (A) Frequency of CD4$^+$ and CD8$^+$ T cells (gated on live TCRβ$^+$ cells) analyzed at D-1 (left panel) in the blood of mice treated with isotype control (Ctrl n=50) or anti-CD4 mAb (n=47); or analyzed at D+27 (right panel) in the blood of mice treated with isotype control (n=25), anti-CD8 mAb (n=21), anti-CD4 mAb (n=22) or both anti-CD4 and anti-CD8 mAb (n=20). Data are from 3 independent experiments. **(B)** Frequency of MHC-II expressing

microglia on day 8 in the hypothalamus of littermate control mice or Orex-HA mice treated with anti-CD4 or control antibodies (n=4-5 per group) from 2 independent experiments. **(C)** Frequency of the hypothalamic clusters in relation to the treatment group. Data are from one experiment involving 4-5 mice per group. **(D)** Comparison of the 3 subsets of transferred $CD8^+$ T cells defined based on PD-1 and TOX expression in the hypothalamus of Orex-HA mice treated with depleting anti-CD4 or control antibodies, on day 30. Data are from 2 independent experiments involving 8-9 individual mice/group. The data from the control group are also shown in Figure S3D. The data were analyzed using one-way ANOVA (B), or Student t-test with Bonferroni correction for multiple testing (D).

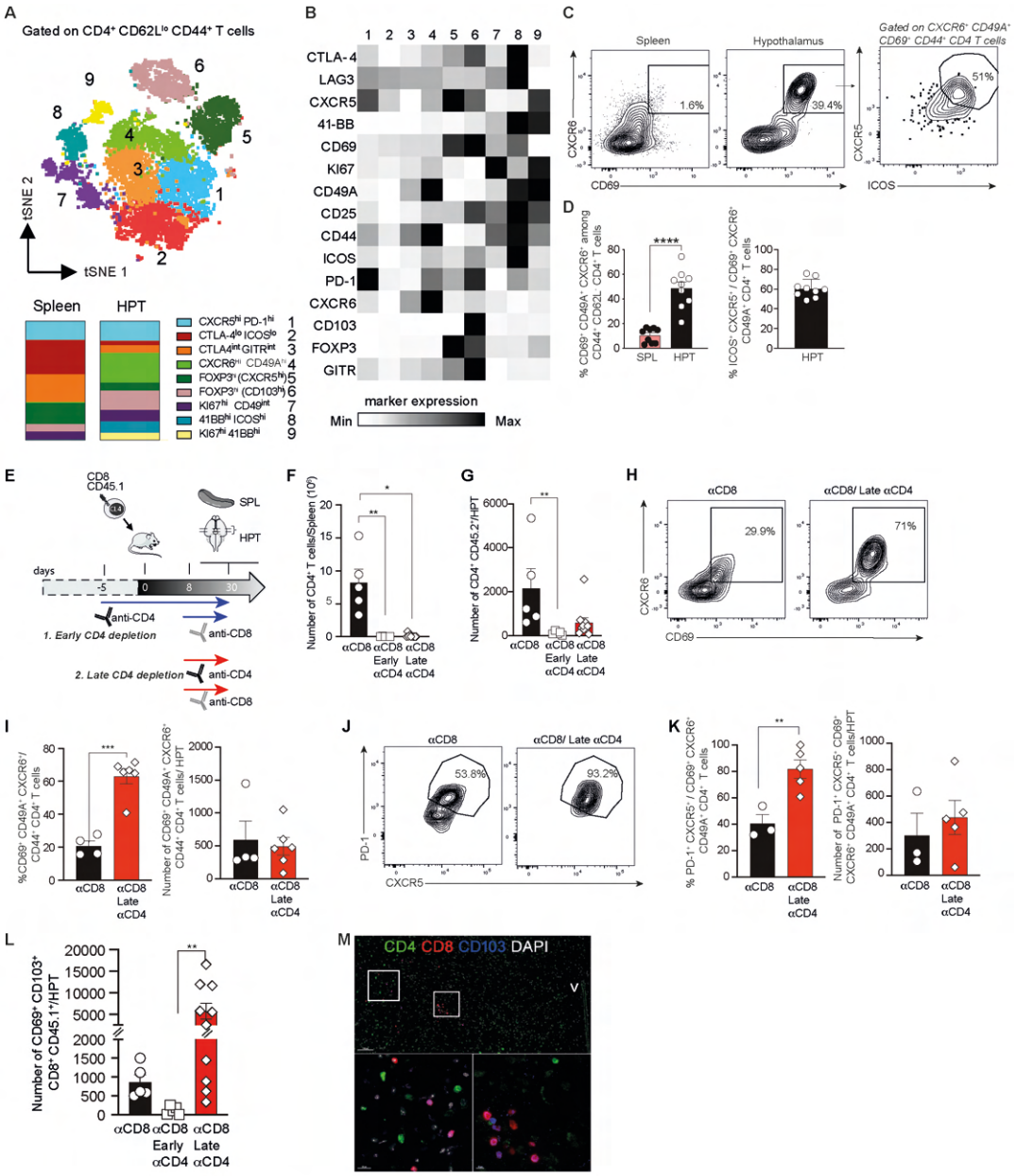

Figure S7. Characterization of hypothalamic CD4$^+$ T cells involved in sustaining tissue-resident CD8$^+$ T cells. (A) tSNE-graph with the cluster overlay of CD44$^+$ CD4$^+$ T cells from the hypothalamus and the spleen analysed by flow cytometry on day 30 post-transfer (top) and their relative representation in the two tissues (bottom). **(B)** Heatmap of the expression of key markers in the 9 identified clusters. **(C, D)** Representative FACS plots on day 30 **(C)** and frequency **(D)** of CD69$^+$ CXCR6$^+$ among CD44$^+$ CD62L$^-$ CD4$^+$ T cells in the spleen and hypothalamus of Orexin-HA mice and the expression of CXCR5$^+$ and ICOS$^+$ by this

hypothalamic subset. Results are from 9 individual mice from 2 independent experiments. **(E)** Schematic experimental design: Orex-HA mice were assigned to one of 3 groups: 1. treatment with depleting anti-CD4 mAb starting 5 days prior to HA-specific $CD8^+$ T cell transfer ('early depletion'), as described in Fig. 7; 2. treatment with depleting anti-CD4 mAb from day 8 onwards ('late depletion'); 3. treatment with an isotype control antibody. In addition, from day 8 onwards, all 3 groups of mice received depleting anti-CD8 mAb. Absolute numbers of $CD4^+$ T cells in the spleen **(F)** and hypothalamus **(G)** at day 30 in the 3 groups of Orex-HA mice (no CD4 depletion; early CD4 depletion; late CD4 depletion; 5 to 10 mice per group) from 2 to 3 independent experiments. **(H)** Representative FACS plots of $CD69^+$ $CXCR6^+$ among $CD44^+$ $CD62L^-$ $CD4^+$ T cells in the hypothalamus of Orex-HA mice treated with anti-CD8 mAb and isotype control or anti-CD4 mAb (late depletion), on day 30. **(I)** Frequency (*left*) or absolute numbers (*right*) of $CD69^+$ $CXCR6^+$ $CD49a^+$ $CD44^+$ $CD62L^-$ $CD4^+$ T cells in the hypothalamus of Orex-HA mice treated with anti-CD8 mAb and control antibodies or anti-CD4 mAb (late depletion) in 1 to 4 pooled mice per data point (n=4-6) from 3 independent experiments. **(J)** Representative FACS plots of PD-1 and CXCR5 expression among $CD69^+$ $CXCR6^+$ $CD49a^+$ $CD44^+$ $CD62L^-$ $CD4^+$ T cells in the hypothalamus of Orex-HA mice treated with anti-CD8 mAb and control antibodies or anti-CD4 mAb (late depletion), on day 30. **(K)** Frequency (*left*) and absolute numbers (*right*) of $CXCR5^+$ $PD\text{-}1^+$ $CD69^+$ $CXCR6^+$ $CD49a^+$ $CD4^+$ T cells in the hypothalamus of Orex-HA mice treated with anti-CD8 mAb and control antibodies or anti-CD4 mAb (late depletion) in 3 to 5 individual mice per group from 2 independent experiments. **(L)** Absolute numbers of transferred ($CD45.1^+$) $CD69^+$ $CD103^+$ $CD8^+$ T cells in the hypothalamus of Orex-HA mice treated with anti-CD8 mAb and control antibodies or anti-CD4 mAb (late and early depletion), on day 30, in 5 to 10 mice per group from 2 to 3 independent experiments. **(M)** Immunofluorescence microscopy identifying $CD4^+$ cells in the vicinity of tissue-resident $CD8^+$ T cells in the

hypothalamus of Orex-HA mice, on day 30 (top; scale bar: 100μm). The two boxed regions are shown at a higher magnification (bottom; scale bar: 20μm); V, blood vessel. Statistical analyses were performed using Mann-Whitney (D), Student t-test (I, K) and Kruskal-Wallis' test with Dunn's correction (F, G, L).

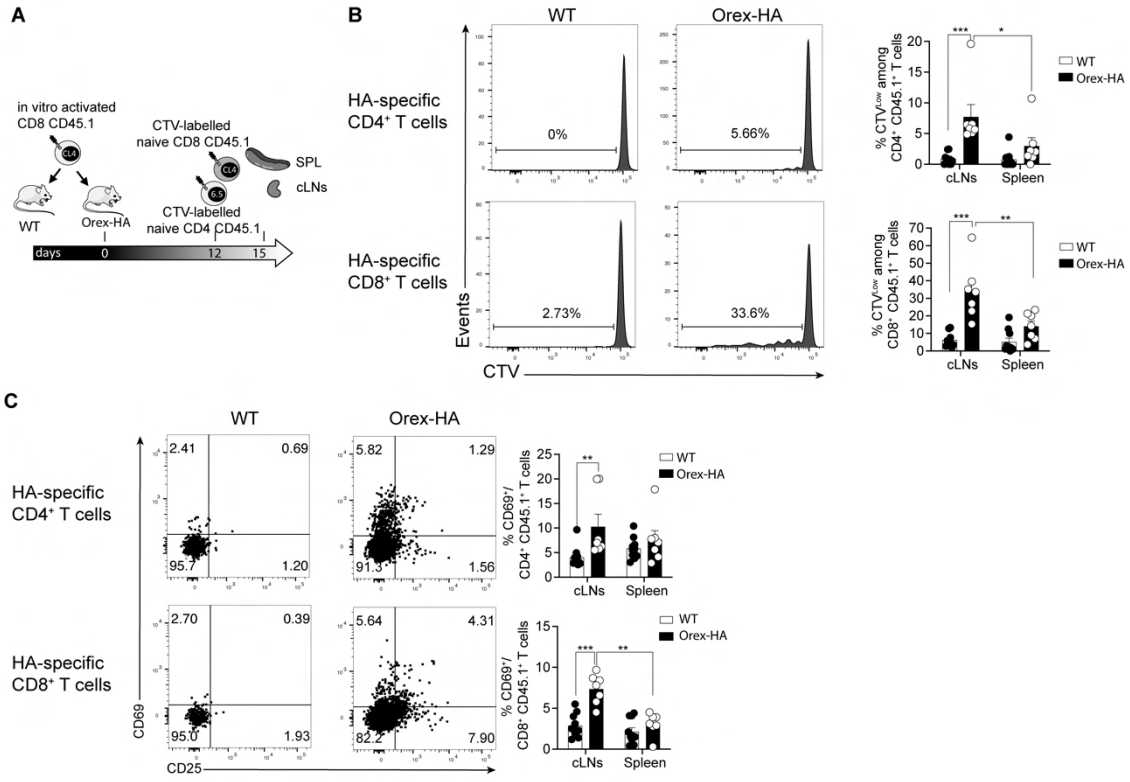

Figure S8. Antigen-specific T cell activation during disease course suggests that neuronal antigens drain in cervical LNs. (A) Schematic experimental design: Orex-HA and littermate control (WT) mice were adoptively transferred i.v. with HA-specific effector $CD8^+$ T cells. On day 12, recipient mice received CTV-labelled naïve HA-specific $CD45.1^+$ CD4 and CD8 T cells from 6.5 and CL4-TCR transgenic mice, respectively. Proliferation and activation of the naïve T cells were analysed in cervical lymph nodes (cLNs) and spleen (SPL) three days later. **(B)** Representative FACS plots (*left*) and frequency (*right*) of CTV^{low} antigen-specific $CD4^+$ (*top*) and $CD8^+$ (*bottom*) T cells in the cLNs and spleen of Orex-HA and WT mice. **(C)** Representative FACS plots (*left*) and frequency (*right*) of $CD69^+$ antigen-specific $CD4^+$ (*top*) and $CD8^+$ (*bottom*) T cells in the cLNs and spleen of Orex-HA and WT mice. Results are from in 7 to 10 mice per group from 2 independent experiments. Statistical analyses were performed using multiple Mann-Whitney's test with Benjamini-Hochberg correction (B,C).

Supplementary tables:

Table S1. Patients' characteristics

Patient	Diagnosis	Age	Sex
1	Limbic/brain stem encephalitis associated with anti-Ma2 antibodies	77	F
2	Paraneoplastic cerebellar degeneration associated with anti-Yo antibodies	66	M
3	Limbic/brain stem encephalitis associated with anti-Ma2 antibodies	77	F
4	Paraneoplastic encephalomyelitis associated with anti-Hu antibodies	83	M
5	Paraneoplastic encephalitis associated with anti-Ri antibodies	59	F
6	Paraneoplastic encephalomyelitis associated with anti-Hu antibodies	72	M
7	Paraneoplastic encephalomyelitis associated with anti-Hu antibodies	74	M
8	Paraneoplastic limbic encephalitis associated with anti-Ma2 antibodies	72	M
9	Paraneoplastic neuronopathy associated with anti-Hu antibodies	71	M
10	Paraneoplastic limbic encephalitis associated with anti-Hu antibodies	65	M

Table S2. Monoclonal antibodies used for flow cytometry

Antibody	Company	Clone	Origin
α4β7 (LPAM1)	BD Pharmingen	DATK32	Rat
BCL-2	eBioscience	10C4	Rat
BST-2	BD Pharmingen	927	Rat
CD103	BD Pharmingen	M290	Rat
CD107a	BD Pharmingen	1D4B	Rat
CD11a (LFA-1)	BioLegend	M17/4	Rat
CD11b	eBiosciences	M1-70	Rat
CD11c	eBiosciences	N418	Hamster
CD127	BD Pharmingen	SB/199	Rat
CD137 (41-BB)	eBiosciences	17B5	Hamster
CD152 (CTLA4)	BD Pharmingen	UC10-4F10-11	Hamster
CD183 (CXCR3)	eBiosciences	CXCR3-173	Hamster
CD185 (CXCR5)	Miltenyi	REA215	Rat
CD186 (CXCR6)	Miltenyi	REA1193	Rat
CD186 (CXCR6)	BioLegend	SA051D1	Rat
CD195 (CCR5)	eBiosciences	HM-CCR5 (7A4)	Hamster
CD195 (CCR7)	BD Pharmingen	4B12	Rat
CD19	BD Pharmingen	1D3	Rat
CD25	BioLegend	PC61	Rat
CD278 (ICOS)	BD Pharmingen	7E.17G9	Rat
CD279 (PD-1)	BioLegend	29F.1A12	Rat
CD357 (GITR)	BD Pharmingen	DTA-1	Rat
CD4	BD Pharmingen	RM4-5	Rat
CD44	eBiosciences	IM7	Rat
CD45.1	BD Pharmingen	A20	Rat
CD45.2	BioLegend	104	Rat
CD49a	BD Pharmingen	Ha31/8	Hamster
CD49d	BD Pharmingen	R1-2	Rat
CD62L	BD Pharmingen	MEL-14	Rat
CD69	BD Pharmingen	H1.2F3	Hamster
CD8a	BD Pharmingen	53-6.5	Rat

CD8b	BD Pharmingen	H35-17.2	Rat
EOMES	eBiosciences	Dan11mag	Rat
FOXP3	eBiosciences	FJK-16s	Rat
GM-CSF	BD Pharmingen	MP1-22E9	Rat
GRANZYME A	eBiosciences	GzA-3G8.5	Rat
GRANZYME B	BioLegend	QA16A02	Rat
IFN-γ	BD Pharmingen	XMG1.2	Rat
IgG2b (Isotype Control)	BD Pharmingen	R35-38	Rat
IL-10	eBiosciences	JES5-16E3	Rat
IL-17A	BD Pharmingen	TC11-18H10	Rat
Ki-67	BD Pharmingen	B56	Rat
Ki-67	eBiosciences	SolA15	Rat
LAG-3	eBioscience	C9B7W	Rat
Ly6a (Sca-1)	BioLegend	D7	Rat
Ly6c	BioLegend	HK1.4	Rat
Ly108 (Slamf6)	BD Pharmingen	13G-3	Rat
MHC-II	BioLegend	M5/114.15.2	Rat
NK-1.1	BioLegend	PK136	Rat
PERFORIN	eBiosciences	eBioOMAK-D	Rat
P2X7R	BioLegend	1F11	Rat
T-Bet	BD Pharmingen	4B10	Rat
TCRβ	BD Pharmingen	H57-597	Hamster
TCR Vβ8.1, 8.2	BD Pharmingen	MR5-2	Rat
Thy1.2	BD Pharmingen	53-2.1	Rat
TIM-3	BD Pharmingen	SD12/TIM-3	Rat
TOX	Miltenyi	REA473	Rat
TNF	BD Pharmingen	MP6-XT22	Rat

Table S3. Antibodies used for immunohistology

Antibody	Origin	Target	Dilution	Reactive fluorophore	Company
Orexin	Rabbit	Orexin A	1:20000 1:6000 1:2000	Cy5 Opal650 DAB	Phoenix Pharmaceuticals #003-30
CD3	Rabbit	Epsilon chain of human CD3	1:500	Opal690	Neomarkers #RM9107-S
CD4	Rabbit	Human CD4	1:250	Opal 520	Cell Signaling # 48274
CD4	Rabbit	Mouse CD4	1:1000	Opal 480	Sino Biological #50143-MO8H
CD8a	Rabbit	Mouse CD8 alpha	1:250 1:2000	Cy2 Opal570	Abcam #ab209775
CD8	Mouse	Human CD8α	1:500	Opal480	DAKO #M7103
GRZMB	Mouse	Human Granzyme B	1:100	Opal520	Neomarkers #MS-1157-S1
GRZMB	Rabbit	Human/mouse granzyme B	1:25	Cy3	Abcam ab4059
CD103	Rabbit	Human Integrin αE	1:5000	Opal570	Abcam #ab129202
CD103	Goat	Mouse Integrin αE/CD103	1:250	Cy3	R&D #AF1990
PD-1	Rabbit	Human PD1	1:150	Opal 570	Abcam #ab137132
PD-1	Rabbit	Human/Mouse PD1	1:50	Cy3	Proteintech #18106-1-AP
CD49a	Sheep	Human Integrin α1/ CD49a	1:250	Cy2	Thermo Fisher #PA5-47763
CD69	Rabbit	Human CD69	1/50	Goat anti-rabbit AF488	Sigma #HPA0505525
BCL2	Mouse	Human BCL2	1/50	Goat anti-mouse IgG1 AF555	Dako Ref:M0887

TOX	Rat	TOX	1/20	Anti-rat HRP +amplification Opal 520	ThermoFisher Ref:14-6502-82 Clone TXRX10
GRZMB	Mouse	Human GrzmB	1/20	Anti mouse HRP +amplification Opal 570	Monosan Ref 7029 Clone GrB-7
CD8	Mouse	Cytoplasmic domain of human CD8α	1:20	Goat anti-mouse IgG1 AF 647	DAKO #M7103
CD8a	Mouse	Human CD8	1/50	Goat-anti mouse IgG2b AF647	Thermo #MA1-80231 Clone 4B11